AAC Accepted Manuscript Posted Online 8 July 2019
Antimicrob. Agents Chemother. doi:10.1128/AAC.00996-19

NU-6027 inhibits growth of *Mycobacterium tuberculosis* by targeting Protein Kinase D and Protein Kinase G

Saqib Kidwai[1], Rania Bouzeyen[2], Sohini Chakraborti*[3], Neha Khare*[4], Sumana Das*[5], Tannu Priya Gosain[1], Assirbad Behura[6], Chhuttan Lal Meena[7], Rohan Dhiman[6], Makram Essafi[2], Avinash Bajaj[4], Deepak Kumar Saini[5], Narayanaswamy Srinivasan[3], Dinesh Mahajan[7] and Ramandeep Singh[1#]

*equal contribution

[1] Tuberculosis Research Laboratory, Vaccine and Infectious Disease Research Centre, Translational Health Science and Technology Institute, NCR Biotech Science Cluster, Faridabad, Haryana- 121001, India.
[2] Institut Pasteur de Tunis, LTCII, LR11 IPT02, Tunis, 1002,Tunisia. Université Tunis El Manar, Tunis, 1068, Tunisia.
[3] Molecular Biophysics Unit, Indian Institute of Science, Bangalore-560012.
[4] Laboratory of Nanotechnology and Chemical Biology, Regional Centre for Biotechnology, NCR Biotech Science Cluster, PO Box # 4, Faridabad, Haryana, India.
[5] Department of Molecular Reproduction, Development and Genetics, Biological Sciences Building, Indian Institute of Science, Bangalore, India.
[6] Laboratory of Mycobacterial Immunology, Department of Life Science, National Institute of Technology, Rourkela, Odisha, India.
[7] Drug Discovery Research Centre, Translational Health Science and Technology Institute, NCR Biotech Science Cluster, Faridabad, Haryana- 121001, India.

#Corresponding author Mailing address: NCR Biotech Science Cluster, 3rd Milestone, Faridabad-Gurugram Expressway. PO Box # 4. Faridabad – 121001.

Running Title: Mechanism of action of NU-6027 against *M. tuberculosis*

Keywords: *Mycobacterium tuberculosis*, NU-6027, apoptosis, serine threonine protein kinases

ABSTRACT

Tuberculosis (TB) is a global health concern and this situation has further worsened due to the emergence of drug resistant strains and failure of BCG vaccine to impart protection. There is an imperative need to develop highly sensitive, specific diagnostic tools, novel therapeutics and vaccines for the eradication of TB. In the present study, a chemical screen of pharmacologically active compounds library was performed to identify anti-mycobacterial compounds. The phenotypic screen identified few novel small molecule inhibitors including NU-6027, a known CDK-2 inhibitor. We demonstrate that NU-6027 inhibits *Mycobacterium bovis* BCG growth *in vitro* and also displayed cross-reactivity with *Mycobacterium tuberculosis* protein kinase D and protein kinase G. Comparative structural and sequence analysis along with docking simulation suggest that the unique binding site stereochemistry of PknG and PknD is likely to accommodate NU-6027 more favorably in comparison to other *M. tuberculosis* Ser/Thr protein kinases. Further, we also show that NU-6027 treatment induces the expression of pro-apoptotic genes in macrophages. Finally, we demonstrate that NU-6027 inhibits *M. tuberculosis* growth in both macrophage and mice tissues. Taken together, these results implicate that NU-6027 may be optimized further for the development of anti-mycobacterial agents.

Introduction

M. tuberculosis is a major global concern with an estimated 10 million incident rates and approximately 1.6 million deaths in 2017 according to the World Health Organisation (WHO) Report (1). Approximately, one-third of the world population is latently infected with *M. tuberculosis*. However, 5-10% of these latently infected individuals develop active disease due to deterioration of their immune response (2). The incidence of TB associated deaths is higher in patients with other communicable and non-communicable diseases (3). The 6-9 months duration of TB chemotherapy and poor patient compliance has led to the emergence of drug-resistant strains. Multidrug drug resistant (MDR)-TB is defined as strains harboring resistance to first line TB drugs, isoniazid and rifampicin (4). MDR-TB that develops additional resistance to fluoroquinolones and one of the injectable second-line TB drug is defined as extensively drug resistant (XDR)-TB (4). The treatment of individuals with MDR-TB and XDR-TB requires combination of second and third line TB drugs that are expensive, more toxic and less effective (5). This duration of medication is between 9-18 months and if the disease progresses into totally drug resistant (TDR)-TB, TB becomes almost untreatable. Therefore, the existing regimen for both susceptible and resistant TB needs to be simplified and shortened.

High throughput screening is the mainstay of drug discovery and has led to the identification of different scaffolds that are currently in different stages of clinical trials (6-9). The current methods of screening for identification of novel scaffolds are either target-based or phenotypic-based. However, small molecules identified through target-based screening have achieved limited success due to lack of translation from *in vitro* enzymatic activity to whole cell activity. In contrast, phenotypic screening has resulted in the discovery of various small molecules that possess a novel mechanism of action. The novel chemical entities identified by phenotypic screening fulfill essential criteria such as cell permeability and provide structures that can be optimized for enhanced potency, better tolerability and pharmacokinetic properties. Phenotypic screening along with sequencing of bacterial genomes isolated from resistant strains has identified several compounds such as bedaquiline, Q203, nitroimidazoles, SQ-109 and Btz-403 in TB drug discovery pipeline (10-15). Among these, bedaquiline and delamanid have been recently approved by FDA for the treatment of individuals with MDR-TB (16, 17). Despite their identification, there is an urgent need to design a regimen that (i) can shorten the duration of therapy, (ii) minimize drug-drug interaction and (iii) is active against drug-resistant and latent bacteria (5, 6, 9).

In the present study, we have performed phenotypic screening using a library of pharmacologically active compounds (Sigma Lopac[1280]) to identify inhibitors against *M. tuberculosis*. Using *M. bovis* BCG as a host strain, we identified the lead compound, NU-6027, 4-cyclohexyl, 2-6-diamino-5-nitrosopyrimidine, that displayed an MIC_{99} value of 1.56 μM. We demonstrate that NU-6027 inhibits autophosphorylation activity associated with Ser/Thr protein kinases (STPKs), protein kinase D (PknD) and protein kinase G (PknG) in a dose-dependent manner. Computational structural studies involving molecular docking simulation, binding site and sequence comparison analysis explain the possible molecular mechanism of specificity of NU-6027 towards PknD and PknG. Further, we show that NU-6027 induces apoptosis and also inhibits the growth of intracellular *M. tuberculosis* in both macrophages and mice model of infection. These findings reinstate the fact that modulation of host and bacterial signaling pathways is an attractive strategy for the design of novel anti-tubercular agents.

Materials and Methods

Strains, growth conditions and compound library screening: *M. tuberculosis* $H_{37}Rv$ and *M. bovis* BCG were cultured in 7H9 medium supplemented with 0.05% tween-80 (v/v), 0.2% glycerol (v/v) and 10% ADS as described previously (18). A compound library comprising 1280 pharmacologically active compounds was purchased from Sigma Aldrich. Preliminary screening was performed against *M. bovis* BCG at a single concentration of 10 μM. In screening experiments, isoniazid was included as a positive control. The identified preliminary hits were re-evaluated for anti-mycobacterial activity and MIC_{99} values were determined as described previously (18). For *in vitro* growth inhibition experiments, early-log phase cultures of *M. bovis* BCG were exposed to different concentrations of either NU-6027 or INH for 4 days or 7 days. At designated time points, 10.0-fold serial dilutions of untreated or drug-treated cultures were prepared and plated on MB7H11 supplemented with 10% OADS.

Chemical synthesis: The experimental details for the synthesis of parent compound, NU-6027, and its derivatives are mentioned in the supplementary information (Supplementary Text). The structural analysis and characterization of the synthesized compounds were performed by $^{1}H/^{13}C$-NMR spectroscopy and mass spectrometry. The corresponding analytical data is provided along with experimental details in the supplementary information (Supplementary Text).

Purification of *M. tuberculosis* STPK enzymes: The expression constructs for PknA, PknB, PknD, PknE, PknF, PknG, PknH, PknJ and PknL were kind gift from Dr. Yogendra Singh, University of Delhi. The overexpression plasmid for PknK of *M. tuberculosis* was a generous gift from Dr. Vandana Malhotra, University of Delhi. *Escherichia coli* Arctic strain was used for overexpression and purification of the recombinant proteins. The expression of recombinant proteins was induced at 18°C, 180 rpm for 18-24 hrs by the addition of IPTG as per standardized conditions. The induced cultures were harvested, resuspended in lysis buffer and STPK's were purified using either Ni-NTA or GST- based affinity chromatography as per manufacturer's recommendations. Purified GST-tagged proteins were concentrated and dialyzed in 1x PBS containing 20% glycerol. Purified $(His)_6$-tagged proteins were dialyzed in buffer containing 50 mM Tris-Cl, pH 8.0, 50 mM NaCl, 0.1 mM DTT, 50% glycerol. The purified and dialyzed recombinant proteins were stored at -20°C till further use.

***In vitro* kinase assays for STPKs:** $(His)_6$-PknA, $(His)_6$-PknB, $(His)_6$-PknD, $(His)_6$-PknJ, $(His)_6$-PknL GST-PknG and GST-PknK enzymes were assayed for autophosphorylation

activity in assay buffer (100 mM PIPES, pH 7.0, 80 mM NaCl and 20 mM $MgCl_2$) containing 1-2μCi of γ^{32}P-ATP for 10-45 minutes at 25°C (19, 20). Autophosphorylation assays of GST-PknE, GST-PknF and GST-PknH were performed in buffer containing 25 mM Tris-Cl, pH 7.4, 5 mM $MgCl_2$, 2 mM $MnCl_2$ and 1 mM DTT for 30 minutes at 37°C (19). The auto-phosphorylation reactions were stopped by the addition of 5x SDS sample loading buffer, resolved on SDS-PAGE and analyzed by phosphor imaging using Typhoon 9210 imager (GE healthcare). To determine the effect of NU-6027 on the activity of STPK's, autophosphorylation assays were performed either in its presence or absence. Image J software was used to determine the extent of autophosphorylation of STPK's *in vitro*.

***In silico* studies:**

A combination of chemoinformatics and bioinformatics based analysis were performed to understand the molecular recognition between NU-6027 and *M. tuberculosis* STPKs. These studies can be broadly classified under three major steps as elaborated below:

(a) Input selection, preparation and analysis of available data: This step pertains to selection and preparation of the appropriate protein-ligand complex structure for docking analysis. The chemical information about NU-6027 was fetched from databases such as PubChem, BindingDB and DrugBank (21-23). The crystal structure of human CDK2 bound to NU-6027 solved at 1.85Å is available in the Protein Data Bank (24) with code: 1E1X (25, 26). NU-6027 is bound to the ATP binding site of human cyclin-dependent kinase 2 (CDK2) in 1E1X, where the DFG loop of the kinase domain is in "in" conformation. This structure has been used for comparative analysis in our study. Our initial choice for experimental structures of STPK's from *M. tuberculosis* which have been used for structural analyses were guided by the following selection criteria which assures the reliability of the structure and subsequent prediction: (i) The available structure of the kinase domain must be solved in holo form (bound to an inhibitor in the ATP binding site of the kinase) with DFG loop in "in" conformation, (ii) There should not be any missing residues in the electron density map of ATP binding site in the protein, and/or (iii) The resolution of the solved structure should be better than 2.5Å. At the time of our study, among the 11 *M. tuberculosis* STPKs, experimental structures of inhibitor bound protein which satisfied our selection criteria were available only for PknG (PDB code: 2PZI, 2.4Å) and PknB (PDB code: 5U94, 2.2Å). While the kinase domain in 2PZI is reported with the DFG loop of the kinase domain in "in" conformation (27), the information on the conformational state of the kinase domain in 5U94 (Wlodarchak, N. *et al.*, to be published according to the Protein Data Bank entry) is not explicitly available. The superimposition of kinase domain from different crystal structures of

Antimicrobial Agents and Chemotherapy

ligand bound PknB complexes (1MRU, 1O6Y and 2FUM) onto the kinase domain of PknB in 5U94 suggested that the DFG loop in the later is in "in" conformation (28-30). This pairwise superimposition was performed using Protein Structure Alignment module in Maestro version 11.01.011 (Schrodinger LLC). The three crystal structures with the PDB codes 1E1X (CDK2), 2PZI (PknG), 5U94 (PknB) were prepared using Protein Preparation Wizard at pH 7.0 (as per the experimental assay condition) (31). The chemical structure of NU-6027 was prepared using LigPrep (Schrödinger, LLC) before docking it into the protein binding site. These prepared structures were used for subsequent structural analysis. In this part of the study, OPLS3 force field was used (32).

To further enhance our understanding on NU-6027's specificity towards PknG and PknD, we extended our computational study to PknA (PDB code: 4OW8, an apo kinase domain of PknA; 2.03Å and PknD) (33). The experimental structure of PknD kinase domain is unavailable and was therefore modelled using PknD surrogate structure (i.e., structure of PknB L145M/V155M/D33L mutant**;** PDB code: 3F69; 2.8Å) as template (34). The PknA structure and PknD model was prepared in the similar way as previous structures were prepared. The chemical structure of NU-6027 was docked into the binding pocket of PknA and PknD model using an advanced version of OPLS3 force-field, *viz*., OPLS3e (35). OPLS3e was also used for building the PknD model for docking studies.

(b) Structural analysis: This analysis of our study can be further sub-classified as under:

(i) *Binding site analysis in the crystal structure of the proteins*: In order to assess the local similarity in the binding site of proteins, pairwise sequence alignment based on the structural superimposition of binding site residues was performed (using binding site and sequence alignment module availed through Schrödinger suite).

(ii) *Prediction of binding pose of NU-6027 in the M. tuberculosis STPKs (PknG, PknB, PknD, and PknA):* To predict the binding pose of NU-6027 in the ATP binding site of the mentioned kinases, we employed flexible binding site – flexible ligand docking simulation using Induced Fit Docking (36) protocol of Schrodinger suite with extended sampling settings (37). The best pose among all the reported output poses was selected based on detailed analysis which involved assessment of retention of crucial interactions between the ligand and hinge residues of the protein kinase domain. Since hydrogen bonds are known to confer specificity to protein-ligand interactions so propensity of occurrence of a hydrogen bond between a particular amino acid residue and the ligand among all the shortlisted poses was calculated (38). Also, the propensity of similar poses (similar with respect to mutual

conformation and orientation of the ligand in the respective protein binding site) predicted throughout the entire set of output poses were taken into consideration for selecting the best representative docked model. Comparative analysis of hydrophobic contacts was performed on the best poses of NU-6027 in respective proteins. The criteria used to detect different non-covalent interactions between the protein and ligand throughout the study is summarized in Table S1. The nitrogen, oxygen, hydrogen, and sulfur atoms of the proteins and ligands are depicted in blue, red, white, and yellow colour, respectively.

(iii) *Comparative modelling*: Comparative structural models of PknD - wild type (WT) sequence was built using PknD surrogate structure (i.e., PknB L145M/V155M/D33L mutant**;** 3F69) as template (34). Chain B of 3F69 has fewer missing residues in the electron density map as compared to chain A. Hence chain B of 3F69 was preferred to be used as template for building of PknD-WT model. The protein chains in 3F69 belong to a PknB construct where two ATP contacting residues have been mutated (L145M and V155M) to mimic PknD's ATP binding site. The other mutation, D33L, is a stabilizing mutation at a site far away from the ATP binding pocket. Prime homology modelling tool was used for model building and only the non-template loop in binding site was refined (39, 40). The quality of the model was assessed using PROCHECK and observed to be satisfactory (data not shown) (41).

(c) Sequence analysis: In order to understand the possible reasons for NU-6027 specificity towards PknG and PknD enzyme, we also performed multiple sequence alignment (MSA) of amino-terminus stretch and kinase domain of all the 11 *M. tuberculosis* STPKs and human CDK2 using MUSCLE (42). The MSA was viewed using ESPript3.0 (43). We also performed Structure based multiple sequence alignments (SBMSA) of kinase domains of *M. tuberculosis* STPKs employing PROMALS3D tool. For SBMSA analysis, experimental structures of the proteins were used wherever available and for remaining STPK's sequences were used (44).

Macrophage experiments: The THP-1 human monocyte cell line was maintained in RPMI 1640 medium containing 10% fetal bovine serum (FBS) as per standard protocols (45). THP-1 monocytes were differentiated by the addition of 20 ng/ml phorbol 12-myristate 13-acetate (PMA) for 48 hrs. Post-differentiation, THP-1 cells were washed twice with 1x-phosphate buffered saline (PBS) and rested for 1 day in RPMI medium. Cell viability assays were performed using cell proliferation reagent, WST-1 as per manufacturer recommendations. For intracellular killing experiments, differentiated THP-1 macrophages were infected with either *M. bovis* BCG or *M. tuberculosis* as previously described (18). Briefly, 24 hrs post-infection, macrophages were overlaid with RPMI medium containing NU-6027 or INH for 4

241 days. At designated time points, macrophages were lysed and 10.0 fold serial dilutions were
242 plated on MB7H11 plates at 37°C for 3-4 weeks. For qPCR analysis, total RNA was isolated
243 from untreated and NU-6027 treated macrophages using Qiagen RNAeasy kit. DNase-I
244 treated RNA was subjected to cDNA synthesis using Superscript III reverse transcriptase.
245 The relative expression levels of gene of interest were calculated after normalization to the
246 expression levels of housekeeping gene, GAPDH as per standard protocol. The list of primers
247 used for qPCR analysis is shown in Table S2.

248 **Analysis of autophagy by fluorescence microscopy:** LC3 puncta formation in untreated and
249 NU-6027 treated macrophages was visualized by confocal microscope as previously
250 described (18). In these experiments, macrophages were incubated with NU-6027 for 6 hrs or
251 24 hrs. In few experiments, 50 nM Bafilomycin A (Baf-A1) was added to macrophages for 3
252 hrs before the completion of experiment. At designated time points, macrophages were fixed,
253 stained and images were captured using confocal scanning laser microscope (Leica
254 Microsystems).

255 **Analysis of apoptosis by flow cytometry:** For detection of apoptosis, mock or infected
256 macrophages with or without NU-6027 treatment were harvested. The macrophages were
257 washed with 1x binding buffer (100 mM HEPES-pH 7.4, 1.4 M NaCl, and 25 mM $CaCl_2$
258 solution) and stained with a mixture of PE-Annexin V and 7-AAD at room temperature. After
259 15 minutes of incubation, 400 µl of 1x binding buffer was added and data was acquired using
260 FACS Caliber (Becton Dickinson). The acquired data was subsequently analysed using
261 FLOWJO 7.6.1 software.

262 **Ethics Statement.** All animal studies were performed in accordance with committee for the
263 purpose of control and supervision on animals (CPCSEA) guideline and approved from the
264 Institutional animal ethics committee of THSTI and ICGEB. All experiments involving *M.*
265 *tuberculosis* were performed in BSL-3 laboratory at Tuberculosis aerosol challenge facility,
266 ICGEB.

267 **Pharmacokinetics and dose tolerance study.** NU-6027 was resuspended in 1%
268 carboxymethyl cellulose to prepare a dosing formulation of 10 mg/ml strength. For drug-
269 tolerability experiments, 100 mg/kg/day of NU-6027 was orally administered for 5
270 consecutive days. Various parameters such as body weight, fur loss, body temperature and
271 mice activity were monitored for 7 days post-drug administration. For pharmacokinetic
272 studies, 4-6 weeks old BALB/c mice were orally administered NU-6027 at a dose of 100
273 mg/kg. At designated time points (3 mice per group) plasma was prepared and subjected to

LC/MS analysis. The detail of pharmacokinetics experiment is provided in the supplementary information (Supplementary Text).

Mouse Infection experiments. 4-6-week-old BALB/c mice were infected with approximately 100 CFU of *M. tuberculosis* via aerosol route. For efficacy studies, 28 days post-infection, rifampicin or NU-6027 was administered orally at a dose of 10 mg/kg or 100 mg/kg, respectively for 5 days a week. At designated time points lungs and spleens were homogenized in normal saline and 10.0 fold serial dilutions were plated on MB7H11 plates at 37°C for 3 – 4 weeks.

Statistical analysis: All statistical analysis was performed using Graph Pad Prism software. The differences between indicated groups were considered significant with $p < 0.05$.

Results

Phenotypic screening results in identification of NU-6027 as the lead compound: *M. bovis* BCG is widely used as a host strain for the screening of small molecule libraries as it can be cultured within a BSL-2 environment and it shares about 99% similarity with *M. tuberculosis* genome (46). Previous studies have demonstrated that hit rates obtained using *M. bovis* BCG are similar to those obtained in *M. tuberculosis* (7, 18, 47). In the present study, we screened a library of pharmacologically active compounds (Sigma Lopac^{1280}) comprising 1280 compounds to identify small molecule antimycobacterial agents. The preliminary screening was performed at a single concentration of 10 μM in duplicates and all plates included DMSO and INH as negative and positive controls, respectively. As expected, no growth inhibition of *M. bovis* BCG was observed in the presence of DMSO while INH yielded complete growth inhibition. We identified 20 primary hits that were able to inhibit the growth of *M. bovis* BCG (Table 1). A number of these compounds have been previously reported to be active against *M. smegmatis*, *M. bovis* BCG and *M. tuberculosis* (48). The structures with already reported activity and those that possessed reactive functional groups were eliminated for future mechanistic studies. Based on our review of available literature, mechanism of action for anti-mycobacterial activity has not been reported in the case of 2-[3-dihydro-(1,3,3-trimethyl-2H-indol-2-ylidene)-1-1propenyl]-3-ethyl-benzothiazolium iodide (AC-93253 iodide), calcimycin (C7522), diphenylene iodonium chloride (D2926) and 4-cyclohexyl, 2-6-diamino-5-nitrosopyrimidine (NU-6027). We next determined IC_{50} values of these small molecules against THP-1 cell line. We did not observe any cytotoxicity in the case of NU-6027 and AC-93253 on THP-1 macrophages at 25 μM and 10 μM, respectively. However, both C7522 and D2926 showed cytotoxicity on THP-1 macrophages at a concentration higher than 2.5 μM and 0.5 μM, respectively. Recently, we have reported that pre-treatment of macrophages with calcimycin induces IL-12 production and also enhances autophagy in P2XR7 dependent manner (45, 49). In concordance with our findings, it has been reported that diphenyleneiodonium chloride displays bactericidal activity against *Staphylococcus aureus* and *M. tuberculosis* (50).

In the following sections, we discuss activity results of NU-6027 against mycobacteria *in vitro*, in macrophages and mice tissues. The chemical structure of NU-6027 consists of a 2,6 diamino pyrimidine linked to cyclohexyl ring by an alkoxy group. We hypothesized that the nitroso group attached to the pyrimidine core of NU-6027 is pharmacologically relevant and critical for the observed *in vitro* activity. To test this

hypothesis, we synthesized the parent compound (a) along with few other truncated analogues and evaluated them for anti-mycobacterial activity *in vitro* (Fig. 1a). As expected, the parent compound (a) displayed MIC_{99} value of 1.56 μM against *M. bovis* BCG. In concordance with our hypothesis, we observed that the removal of NO group (b) completely abolished the *in vitro* activity associated with NU-6027 (Fig. 1a). The other synthesized truncated analogues (c and d) were also inactive in our *in vitro* activity assays (Fig. 1a). In conclusion, this limited analog screening did highlight the importance of nitroso group for the anti-mycobacterial activity of NU-6027. Next, we determined the mode of *M. bovis* BCG growth inhibition by NU-6027. We observed that exposure to 10x MIC_{99} concentration of NU-6027 for 7 days reduced the viable counts by approximately 4.5 folds (Fig. 1e, *$p<0.05$). As expected, 70.0-fold reduction was seen in 10x MIC_{99} concentration of INH-treated cultures after 7 days of exposure (Fig. 1e, **$p<0.01$). We also demonstrate that NU-6027 is able to inhibit the *in vitro* growth of *M. bovis* BCG in both dose and time dependent manner (Fig. 1f, *$p<0.05$ and **$p<0.01$).

NU-6027 inhibits PknD and PknG enzymes from *M. tuberculosis*: The substituted pyrimidine ring of NU-6027 mimics the adenine ring of ATP and is involved in interactions with critical residues in the crystal structure of CDK2 (25). Since bacterial and mammalian kinases possess conserved architecture of ATP binding site in their kinase domain, we hypothesized that NU-6027 might be able to target multiple cellular events regulated by *M. tuberculosis* STPK's. Numerous studies have shown that STPK's undergoes autophosphorylation to initiate phospho-mediated signaling (51). To test this hypothesis, we next evaluated the ability of NU-6027 to inhibit autophosphorylation activity associated with *M. tuberculosis* STPK's. For *in vitro* autophosphorylation assays, *M. tuberculosis* STPK's were purified as either $(His)_6$-tagged proteins (in the case of PknA, PknB, PknD, PknJ and PknL) or as GST-tagged proteins (in the case of PknE, PknF, PknG, PknH and PknK), concentrated, dialysed and stored in -80°C till further use (Fig. S1). Next, we determined the effect of NU-6027 on the autophosphorylation activity of all purified STPK enzymes except PknI (Fig. 2). We observed that NU-6027 inhibited autophosphorylation activity associated with both PknD and PknG in a dose-dependent manner (Fig. 2a and 2b). As shown in Fig. 2a, we demonstrated that NU-6027 did not affect the auto-phosphorylation activity associated with other tested STPK's (PknA, PknB, PknE, PknF, PknH, PknJ, PknK and PknL). These results implicate that NU-6027 specifically inhibits PknD and PknG auto-phosphorylation without affecting other STPK's.

Comparative structural analyses to understand the specificity of NU-6027 towards PknG and PknD: As discussed in the Materials and methods section, initially, the crystal structures of PknB (5U94) and PknG (2PZI) were selected for detailed computational analysis. The structure of PknB in 5U94 served as a representative among the 8 *M. tuberculosis* STPKs (PknA, PknB, PknE, PknF, PknH, PknJ, PknK, and PknL) which did not show any inhibitory response in the presence of NU-6027. The available structure of PknG and PknB provided an opportunity to investigate the possible reasons for NU-6027 specificity towards PknG over PknB. The structure of human CDK2 bound to NU-6027 (PDB code: 1E1X) helped in understanding the critical interactions which are essential to elucidate kinase activity inhibition by NU-6027. The molecular docking studies were later extended to PknD and PknA.

(i) Binding site analysis of PknG and PknB: Pairwise structure-based binding site sequence comparison between PknB (5U94) and PknG (2PZI) revealed that while the root mean square deviation (RMSD) of C_α atoms of the aligned residues is 1.5Å, the sequence identity between the binding site residues is 48% (Fig. S2a, b). These observations suggest that the binding sites of these proteins differ in both composition and conformation of the constituting residues. Such dissimilarities of binding site structures might confer a varying response by different STPKs in recognition of NU-6027. To understand the probable binding mode of NU-6027 to PknG and PknB, we next performed molecular docking analysis.

(ii) PknG-NU-6027 induced fit docking analysis: The output poses from the induced fit docking (36) experiments were manually scrutinized and selected for further analysis as described in Materials and methods section. We observed that in 50% and 38% of the selected poses from PknG:NU-6027 experiment, the 5-nitroso and 6-amino substituent of NU-6027 are engaged in hydrogen bond formation with the main chain of the hinge residues: Val235 and Glu233, respectively. Overall, 31% of the poses are engaged in hydrogen formation with both Val235 and Glu233. The predicted pose of NU-6027 in PknG from our docking experiments is similar to the bound pose of AX20017, a known PknG specific inhibitor (2PZI), with respect to placement of the hydrophobic and adenine-mimetic rings of the two compounds (Fig. S2c, d). Interestingly, AX20017 as well as ATP analogues (PDB code: 4Y0X, 4Y12) are also involved in hydrogen bond interactions with these amino acid residues (52). Their equivalent residues, Glu81 and Leu83 in the case of CDK2 and Glu93 and Val95 in the case of PknB (PDB code: 1O6Y, 1MRU, 5U94) are also known to participate in hydrogen bond formation with their respective inhibitor or the adenine ring of ATP or ATP analogues (28, 30). Previously, it has been shown that pyrimidine and purine

analogues which failed to engage Glu81 of CDK1/2 in hydrogen bond formation are unable to inhibit these enzymes (25). However, pyrimidine and purine analogues that were unable to form hydrogen bond with Leu83 displayed reduced inhibition of activity associated with CDK1/2 enzymes (25). In addition to these interactions, we also observed that the amino group at 6th position of the pyrimidine ring of NU-6027 forms hydrogen bond with the main chain of Ile292 in 92% of PknG:NU6027 shortlisted poses. The Ile292 residue is unique to the binding site of PknG and is substituted with methionine and alanine in PknB and CDK2, respectively (Fig. S3). Interestingly, in the top ranked pose, NU-6027 is involved in hydrogen bonding with Glu233, Val235 and Ile292 of PknG. In addition, the 2-amino substituent in the pyrimidine ring of NU-6027 is also involved in hydrogen bond formation with the side chain of Asp293 (Fig. 3a). This Asp293 is part of the conserved DF(/L)G motif near the activation loop of kinases. In addition to the conserved residues, NU-6027 also forms hydrophobic interactions with six non-conserved residues which include Ile165, Val179, Ile292 and Gly236 from the kinase domain and Ile87 and Ala92 in the amino-terminus region (Fig. 3a**)**. These residues have also been demonstrated to be important for interactions between AX20017 and PknG binding site (27).

(iii) PknB-NU-6027 induced fit docking analysis: Analysis of the induced fit docking poses of NU-6027 in PknB showed that the functional residues such as Glu93 and Val95 are not involved in hydrogen bond formation with NU-6027. Previously, it has been shown that inhibitor such as G93 forms hydrogen bond with residues such as Glu59, Lys40 and Asp156 (Wlodarchak, N. *et al.*, to be published according to the Protein Data Bank entry). However, these residues are not involved in hydrogen bond formation in the predicted PknB:NU-6027 induced fit docked poses (Fig. 3b). The best representative induced fit docked pose of NU-6027 in PknB binding site is predicted to be involved in hydrogen bonding with Leu17 and Ala142 (which are not known to be crucial for enzyme inhibition).

(iv) PknD-NU-6027 induced fit docking analysis: Analysis of the induced fit docking poses of NU-6027 in PknD-WT model showed that the two hinge residues, Arg93 and Ile95 are involved in hydrogen bond formation with NU-6027 in 9% and 91% of the poses, respectively. In 9% of the overall poses, both Arg93 and Ile95 are involved in hydrogen bond formation with NU-6027. Additionally, NU-6027 is also involved in hydrogen bond formation with main chain of Gly97 in 82% of the poses. The best representative pose of NU-6027 in PknD binding site is predicted to be involved in hydrogen bonding with Ile95 and Gly97 (Fig. 3c).

(v) PknA-NU-6027 induced fit docking analysis: Analysis of the induced fit docking poses of NU-6027 in PknA showed that the two hinge residues, Glu96 and Val98, are involved in hydrogen bond formation with NU-6027 in some of the poses. However, both these residues are involved in hydrogen bond formation with NU-6027 in only 0.06% of the overall poses. The best representative pose of NU-6027 in PknA binding site is predicted to be involved in hydrogen bond formation with Glu96 and Asp159 (Fig. 3d). Contrary to other docking simulations, we also noticed that a part of the hydrophobic component (few carbon atoms of the cyclohexyl ring) of NU-6027 in PknA binding site is solvent exposed in all the predicted poses. This might be the reason for inability of NU-6027 to bind and inhibit PknA autophosphorylation activity.

(vi) Comparative analysis of binding mode of NU-6027 in PknG with other studied kinases: The docked poses of NU-6027 from PknG:NU-6027 and PknB:NU-6027 predicted complexes were overlaid on to the bound pose of NU-6027 obtained from the crystal structure of human CDK2 (Fig. 4a). We noticed that the pyrimidine ring of NU-6027 in CDK2 and PknG occupies almost equivalent regions in their respective protein binding pocket. Although the ligand atoms involved in pyrimidine ring mediated interactions with PknG and CDK2 differ but the crucial interactions with the conserved ATP binding site are retained (Fig. 4a). We observed a displacement of almost 80° between the cyclohexyl ring of NU-6027 in PknG as compared to that in CDK2. Consequently, the cyclopropyl ring mediated hydrophobic contacts between NU-6027 and PknG or CDK2 are distinct. As shown in Fig. 4a, the docked pose of NU-6027 in PknB is such that the pyrimidine and cyclohexyl rings are almost flipped by 180° with respect to the bound pose of the ligand in CDK2 which would prohibit the establishment of relevant interactions between PknB and NU-6027. Interestingly, in PknD:NU-6027, the pyrimidine ring of NU-6027 is placed near to the hinge region similar to that observed in PknG:NU-6027 predicted complex (Fig. 4b). These observations suggests that crucial interactions required for enzyme inhibition are most likely to be retained in the case of PknD. Surprisingly, the best representative pose of NU-6027 in PknA binding pocket also resembles the pose of NU-6027 in PknG (Fig. 4b). However, in only 0.06% of the total PknA poses (in comparison to 31% in the case of PknG), both functional residues in the hinge region are involved in hydrogen bond formation with NU-6027. Moreover, we observed that the hydrophobic cyclohexane ring of NU-6027 is solvent exposed in all the PknA:NU-6027 poses (Fig. 4c). On the contrary, the corresponding atoms of the cyclohexane ring of NU-6027 in PknG is shielded by a set of unique residues from the kinase domain (Gly236) and the N-terminal segment (Ile87 and Ala92) (Fig. 4d). Taken

452 together, these observations are in concordance with our experimental results showing that
453 NU-6027 possesses dual specificity against PknD and PknG and is unable to inhibit the
454 autophosphorylation activity of PknA and PknB enzyme *in vitro*.
455 **Sequence analysis of PknG with other STPKs:** Our docking analysis revealed that the
456 predicted binding site of NU-6027 in PknG comprises of unique amino acid residues (Ile165,
457 Val179, Gly236, Ile292, Ile87 and Ala92) that are absent in PknB binding site. In
458 concordance, similar observations are also noted in the comparative sequence analysis of
459 PknG with other *M. tuberculosis* STPKs (Fig. S3). Sequence analysis of 491 human protein
460 kinases published earlier revealed that the frequencies of occurrence of Ile165, Val179,
461 Gly236 and Ile292 amino acid residues surrounding the PknG binding site are 0.037, 0.065,
462 0.088 and 0.077, respectively. Further, the combination of these four residues is not observed
463 in the sequence of any other human kinases (27, 53). Additionally, Ile87 and Ala92 residues
464 lying in the amino-terminal peptide stretch are also specific to the ligand-binding pocket of
465 PknG. Previously, it has been demonstrated that Ala92 and Ile87 are essential in the binding
466 of PknG specific inhibitors (27). Further, SBMSA analysis revealed that arrangement of two
467 residues, Ser99 and Val155, in PknD binding site might be important for NU-6027 specificity
468 (Fig. S4). The residues corresponding to Val155 of PknD are not branched chain amino acids
469 in other STPKs except for PknG, PknE and PknH. The corresponding residues are Ile292 in
470 PknG, Val156 in both PknE and PknH sequences (Fig. S4). Also, our detailed SBMSA
471 analysis revealed that only PknG and PknK contain a serine residue (Ser293 in PknG and
472 Ser110 in PknK) equivalent to Ser99 in PknD (Fig. S4).
473 **NU-6027 enhances apoptosis in *M. bovis* BCG infected macrophages:** *M. tuberculosis* is a
474 highly successful intracellular pathogen by virtue of its ability to inhibit several antimicrobial
475 mechanisms of the host. These include pathways such as generation of reactive oxygen and
476 nitrogen species, phagosome-lysosome fusion, autophagy and apoptosis (54, 55). Several
477 studies have shown that augmentation of host defensive pathways such as autophagy results
478 in inhibition of the growth of intracellular mycobacteria (56). Thus, we next determined the
479 ability of NU-6027 to induce autophagy in THP-1 cells. We did not observe any significant
480 increase in LC3-puncta formation in NU-6027 treated THP-1 cells at both 6 hrs and 24 hrs
481 post-treatment (Fig. S5a). As expected, a significant increase in LC3-puncta formation was
482 observed in calcimycin treated macrophages (Fig. S5b, $^{**}p<0.01$). We also measured
483 autophagy flux in NU-6027 treated THP-1 cells by inhibiting phagosome-lysosome fusion in
484 the presence of Baf-A1. However, we did not observe any differences in LC3 puncta
485 formation in NU6027 treated THP-1 cells in the absence or presence of Baf-A1 (Fig. S5c and

S5d). These observations demonstrate that NU-6027 is unable to induce autophagy in THP-1 macrophages.

In addition to autophagy, apoptosis is another major mechanism elicited by the macrophages to limit multiplication of intracellular pathogens like *M. tuberculosis* (57). Previously, it has been shown that NU-6027 inhibits CDK1/2, ATR enzymes and induces apoptosis in ovarian cancer cell lines (25, 58, 59). Hence, we next sought to investigate the ability of NU-6027 to enhance apoptosis of *M. bovis* BCG-infected macrophages, 24 hrs post-treatment (Fig. 5a). We found that the percentage of Annexin-V positive cells was significantly enhanced in *M. bovis* BCG-infected macrophages after treatment with NU-6027. The percentage of Annexin-V positive cells in NU-6027 treated and BCG infected macrophages was 35.6% and 33.6%, respectively (Fig. 5a). As shown exposure to NU-6027 enhanced percentage of apoptosis in *M. bovis* BCG infected macrophages to 55.6% (Fig. 5a). Previous studies have reported that enhanced apoptosis of mycobacteria infected macrophages is associated with upregulation of pro-apoptotic genes (60). In an attempt, to better understand the mechanism of induction of apoptosis by NU-6027, we quantified the transcript levels of apoptosis related genes such as NOXA and TNF-α in NU-6027 treated macrophages (Fig. 5b). In comparison to non-treated macrophages, NOXA transcript levels were increased by approximately 6.0-fold in NU-6027 treated macrophages (Fig. 5b, *$p<0.05$). It has been reported that NOXA activation results in upregulation of signaling pathways, which eventually results in mitochondria activation (61). Hence, we sought to evaluate the expression of mitochondria derived pro-apoptotic proteins, apoptosis induced factor (AIF) and endonuclease G (EndoG) in NU-6027 treated THP-1 macrophages. As shown in Fig. 5b, we observed that the transcript levels level of AIF and EndoG were increased by approximately 3.0 and 2.0 folds, respectively in NU-6027 treated THP-1 cells. Interestingly, we also observed that NU-6027 increased the transcription of TNF-α by approximately 7.0 folds suggesting the activation of apoptosis pathway (Fig. 5b, *$p<0.05$). These observations indicate that NU-6027 is a potent inducer of apoptosis in macrophages by activating these pathways.

NU-6027 is able to inhibit the growth of *M. bovis* BCG and *M. tuberculosis* in THP-1 macrophages: Previously, it has been reported that PknG is secretory in nature and promotes survival of *M. tuberculosis* in macrophages by inhibiting phagosome-lysosome fusion (62-64). Previous studies have shown that compounds modulating host apoptosis and targeting PknG are promising anti-mycobacterial agents (27, 64-71). Since NU-6027 possessed both these activities, we sought to assess its anti-mycobacterial activity in THP-1 macrophages

infected with either *M. bovis* BCG or *M. tuberculosis*. Based on CFU enumeration, we observed that NU-6027 inhibited growth of both intracellular *M. bovis* BCG and *M. tuberculosis* (Fig. 5c and 5d). In THP-1 macrophages, pre-treatment with INH reduced the bacterial loads by approximately 93% and 86% in the case of *M. bovis* BCG and *M. tuberculosis*, respectively (Fig. 5c and 5d, **$p<0.01$). In comparison, treatment with NU-6027 inhibited the growth of *M. bovis* BCG and *M. tuberculosis* by 78.1% and 80.1%, respectively (Fig. 5c and 5d, *$p<0.05$).

We next determined whether Z-VAD-FMK, an inhibitor of apoptosis abrogates intracellular killing activity of *M. bovis* BCG by NU-6027 (72). As shown in Fig. 6a, we observed that pretreatment with Z-VAD-FMK reduced the percentage of apoptosis induced in *M. bovis* BCG infected macrophages upon NU-6027 treatment by 50%. In order to further dissect the role of induction of macrophage apoptosis and intracellular killing, we also demonstrate that preincubation of macrophages with Z-VAD-FMK reduced the killing activity of NU-6027 against intracellular mycobacteria (Fig. 6b, *$p<0.05$). These results reaffirm previous observations that augmentation of apoptosis in infected macrophages results in reduced intracellular mycobacterial survival.

NU-6027 is well tolerable in BALB/c mice: Next, we performed an oral single dose pharmacokinetic study of NU-6027 in BALB/c mice to determine plasma exposure of lead compound NU-6027. For pharmacokinetic studies, 4-6 weeks old BALB/c mice were orally administered NU-6027 at a dose of 100 mg/kg using 1% CMC as dosing vehicle. Animals were bled under mild anesthesia at designated time points and LC/MS analysis was performed to determine different parameters such as AUC, C_{max}, T_{max} and $T_{1/2}$ as described in Materials and methods. We observed that NU-6027 was orally bio-available with AUC of 1.5 μM and $T_{1/2}$ of 0.96 hours (Fig. 7a and 7b). Next, we performed dose tolerance study to determine an appropriate dose for efficacy experiments in infected animals. For drug tolerance experiment, healthy BALB/c mice were dosed with 100 mg/kg of NU-6027 for 5 consecutive days and monitored for various health parameters. We observed that daily administration of NU-6027 did not alter either body weight or food intake when compared to the control group (data not shown). The animals from NU-6027 treated group and control group were sacrificed at the end of this study and vital organs (liver, heart and kidney) were visually inspected. The tissues from NU-6027 treated mice did not show any discoloration or change in morphology of the vital organs when compared to controls (data not shown). These

results indicate that a dosage of 100 mg/kg for NU-6027 in BALB/c mice is well tolerable and suitable for an efficacy experiment to establish the required proof of concept studies.

NU-6027 inhibits the growth of *M. tuberculosis* in mice tissues: For efficacy experiments, female BALB/c mice were infected with single cell suspension of log-phase cultures of *M. tuberculosis* via aerosol route. After 4 weeks of infection, both NU-6027 and Rif were orally administered at a dose of 100 mg/kg and 10 mg/kg, respectively for either 2 weeks or 4 weeks. As shown in Fig. 7c, in comparison to untreated control group, reduction in lung bacillary load was observed in mice treated with either Rif or NU-6027. We observed that at 4 weeks post-treatment, lung bacillary loads in control, Rif-treated and NU-6027 treated mice were $\log_{10}$ 5.42, $\log_{10}$ 3.90 and $\log_{10}$ 4.52, respectively (Fig. 7d, *$p<0.05$ and ***$p<0.001$). A similar reduction in splenic bacterial loads was also noticed in these mice after 4 weeks of treatment. We observed that 4 weeks post-treatment, the splenic bacillary load in Rif and NU-6027 treated mice was reduced by approximately 90.0-100.0 fold in comparison to the bacterial loads in spleens of untreated mice (Fig. 7d, ***$p<0.001$). At 2 weeks post-treatment, Rif alone reduced lung bacillary loads by 40.0 fold in comparison to untreated animal, while oral administration of NU-6027 reduced the bacterial loads in lungs by approximately 8.0 fold (Fig. 7c, *$p<0.05$ and ***$p<0.001$). In concordance, 2 weeks treatment of mice with Rif or NU-6027 reduced the splenic bacillary loads by 10.0 fold and 5.0 fold, respectively, in comparison to the untreated mice (Fig. 7d, *$p<0.05$). Taken together, these studies suggest that the dual mechanism of augmenting host apoptosis and inhibiting PknD and PknG STPK's from *M. tuberculosis* is a promising strategy to kill *M. tuberculosis* in macrophages and mice tissues.

Discussion.

Phenotypic screening has resulted in identification of many scaffolds that are in clinical pipeline (6, 8). Despite the availability of increasing number of preclinical candidates, there is still a need to develop more drugs with a novel mechanism to tackle this global epidemic. In the present study we have performed phenotypic assays to screen a library of pharmacology active compounds (Sigma Lopac[1280]) for identification of anti-mycobacterial compounds. We identified 20 compounds that possessed anti-mycobacterial activity and selected NU-6027 for further evaluation in this study. The other identified molecules were given low priority, either due to their previously reported activities or because of cellular cytotoxicity or structural features. Here, we report that NU-6027 inhibited *M. bovis* BCG growth in a dose dependent manner and the nitroso functional group is essential for the *in vitro* activity. These observations are in concordance with previous studies where the Nitro functional group has been shown to be important for anti-mycobacterial activity associated with various scaffolds (10, 11, 18).

NU-6027 is a potent inhibitor of various kinases such as CDK1/2, ATR and DNA-PK with Ki values of 1.3/2.5 μM, 0.4 μM and 2.2 μM, respectively (25, 73). Since protein kinases share similar structural fold in their active sites, we hypothesized that NU-6027 might also be able to inhibit STPK's from *M. tuberculosis.* In support of our hypothesis, we observed that NU-6027 inhibits autophosphorylation activity associated with PknD and PknG in a dose-dependent manner. Intriguingly, the lead compound failed to inhibit autophosphorylation activity associated with other STPK's including PknA and PknB. Previously, structures with amino-pyrimidine scaffolds have been reported as inhibitors of PknB in addition to human kinase (74, 75). Next, to understand the specificity of NU-6027, detailed computational structural as well as sequence analyses were performed. We noticed that in the modeled PknG:NU-6027 complex, NU-6027 is interacting with functional residues, which are known to be involved in ATP binding. However, in the case of PknB, interactions with these functional residues are not observed in any of the predicted poses of PknB:NU-6027. An in-depth comparative analysis of the docked models revealed that apart from conserved kinase domain residues, a set of six unique residues (Ile165, Val179, Gly236, Ile292, Ile87 and Ala92) surrounding the PknG binding site are also be involved in non-covalent interactions with NU-6027. These residues are absent in PknB binding site. Comparative sequence analysis of 11 STPKs from *M. tuberculosis* confirmed that these residues are present only in PknG and are absent in the sequences of other *M. tuberculosis*

608 STPKs. The combination of these residues is also absent in the sequences of human kinases
609 as mentioned earlier. We also observed that 2-amino substituent in the pyrimidine ring of
610 NU-6027 is involved in hydrogen bond formation with the side chain of Asp293 in PknG.
611 Moreover, the binding mode of NU-6027 in PknG is such that its cyclohexyl ring can interact
612 with a non-conserved hydrophobic pocket which is distinct from CDK2:NU-6027 crystal
613 structure. These unique interactions would provide the guiding steps for further optimization
614 of potency and specificity of NU-6027 towards PknG. However, these interactions are solely
615 based on *in silico* studies and demand further experimental validations. Such validations
616 could aid in estimating the risk-to-benefit ratio for taking NU-6027 forward as an effective,
617 safe, and novel anti-tubercular lead molecule.

618 Several studies have shown that modulation of host and bacteria signaling pathways
619 is an attractive target to combat TB (76). To establish a successful infection, *M. tuberculosis*
620 relies on signal transduction pathways such as TCS, STPKs to sense extracellular signal and
621 adapt in the host through a cascade of protein phosphorylation and dephosphorylation events
622 (76, 77). Among STPKs PknA, PknB and PknG are required for intracellular growth and
623 survival (76). Both PknA and PknB are essential for *M. tuberculosis* growth *in vitro* (78, 79).
624 PknG has also been reported to be involved in *M. tuberculosis* survival in macrophages
625 because of its role in glutamate metabolism or via modulation of host signaling pathways
626 such as phagosome-lysosome fusion (62, 80, 81). In addition to these functions, PknG is also
627 required for *M. tuberculosis* growth during stationary phase, biofilm formation and establish
628 infection in guinea pigs and mice (64). Therefore, targeting PknG by NU-6027 would result
629 in inhibition of bacterial metabolism and phagosome-lysosome fusion to promote
630 intracellular killing.

631 In another study it has been shown that PknD is an essential regulator of osmo-
632 sensory signaling pathway and peptidoglycan architecture (82). In addition, PknD is also
633 required for *M. tuberculosis* growth in phosphate poor growth conditions and pathogenesis
634 (83). The results of PknD:NU-6027 docking coupled with sequence analysis revealed that
635 Val155 preceding the aspartic acid residue in DF(/L)G motif might be crucial for binding of
636 NU-6027 to PknD. Interestingly, the corresponding amino acid residue is Ile292 and Met155
637 in the case of PknG and PknB, respectively. We hypothesize that the straight and bulky side
638 chain of methionine might hinder the binding of NU-6027 in PknB binding site whereas
639 branched and comparatively shorter chain residues would provide optimum contacts
640 facilitating binding of NU-6027 in the case of PknD and PknG. In concordance, it has been
641 demonstrated that Met155 hinders the binding of the inhibitor KT5720 in PknB, thus

642 contributing towards the specificity of KT5720 against PknD in comparison to PknB (34).
643 Another interesting similarity between PknG and PknD is the presence of a serine residue at
644 equivalent positions, 239 and 99, respectively. All other *M. tuberculosis* STPKs (except
645 PknK) has a bulkier amino acid residue at this position. Therefore, we speculate that the
646 presence of a serine residue in combination with branched chain residue at position 155 of
647 PknD (292 of PknG) might provide the specificity of NU-6027 towards PknG and PknD.
648 Interestingly, on the hand, our analysis hints that favorable accommodation of NU-6027 in
649 PknA and PknB binding pocket is unlikely which corroborates with our experimental
650 findings as explained earlier.

651 Apoptosis of infected macrophages is considered as an important innate defense
652 mechanism that enables the direct killing of intracellular mycobacteria by destroying its
653 habitat and stimulating an efficient adaptive immune response (65-67). Several studies have
654 shown that virulent strains of *M. tuberculosis* disrupt host apoptotic pathways in order to
655 enhance their intracellular survival (84). In our study, NU-6027 significantly enhanced the
656 apoptosis of *M. bovis* BCG infected THP-1 macrophages. We also show that NU-6027
657 treatment of macrophages results in induction of apoptosis related genes such as NOXA and
658 TNF-α. We also observed that NU-6027 mediated inhibition of PknD, PknG enzymes and
659 apoptosis induction reduced survival of *M. tuberculosis* in mice tissues. These observations
660 are in concordance with the current notion that apoptosis of the infected phagocytes prevents
661 mycobacteria to establish a suitable niche for its long-term survival in the host (65). In
662 agreement, other studies have also identified PknG specific inhibitors such as AX20017,
663 amino-pyrimidine derivatives, AZD7762, R406, R406f, CYC116 and Sclerotiorin as
664 promising antimycobacterial agents (27, 68-71, 76). Taken together, we show for the first
665 time that small molecule targeting PknD and PknG has no side effects and inhibits bacterial
666 growth in lungs and spleens of infected mice.

667 Numerous reports have demonstrated that supplementation of anti-TB therapy with a
668 modulator of the host responses is an effective strategy against drug-resistant strain and also
669 reduces the risk of relapse (6). Our experimental finding that NU-6027 is able to inhibit the
670 growth of intracellular *M. tuberculosis* in mice model suggests that it can be used as an
671 adjunct to TB therapy. Since active TB patients also show a defect in monocytes and
672 macrophages apoptosis, NU-6027 can also be proposed as an apoptosis inducer during TB
673 chemotherapy (85, 86). Developing novel molecules, that are able to unleash the
674 mycobacteria-mediated blocking of macrophage apoptosis, might prove useful as a host-

675 directed strategy against TB. The observed intracellular activity underscores the potential for
676 NU-6027 and similar STPK inhibitors or apoptosis inducers to be developed as effective *M.*
677 *tuberculosis* therapeutics. These compounds would provide suitable starting points to further
678 develop these scaffolds using medicinal chemistry approach.

Authors Contributions

RS planned the study and designed experiments. SK and TP performed microbiology and animal experiments. RB and AB performed macrophage experiments. SC conducted the *in silico* experiments and analyses. NK and CLM performed chemical synthesis. SD performed autophosphorylation assays. RS, DM, AB, ME, DS, RD and NS analysed the results. RS and SC wrote the manuscript with inputs from other authors.

Acknowledgments

The authors acknowledge the funding received from THSTI and Department of Biotechnology, Govt. of India (BT/IN/Indo-Tunisia/01/2014). RS is a recipient of Ramalingaswami fellowship and National Bioscience Award from Department of Biotechnology. This research is also supported by Indian Institute of Science-Department of Biotechnology partnership program to NS who is also a J. C. Bose National Fellow. Support to NS for infrastructural facilities from Fund for Improvement of Science and Technology infrastructure (FIST), DST and Centre for Advanced Structures (CAS), University Grants Commission (UGC) is also acknowledged. Support to RD (EMR/2016/000048, EEQ/2016/000205 and DST/INSPIRE/Faculty award/2014/DST/INSPIRE /04/2014/01662) is acknowledged. The authors also thank Prof. R. Sowdhamini for her generous support in providing access to Schrödinger suite of programs. We thank the technical staff of Tuberculosis aerosol challenge facility, ICGEB for their help during animal experiments. RB acknowledges Department of Science and Technology, India and FICCI for providing C.V. Raman International fellowship. SC, TP and SM are thankful to DST-INSPIRE, DBT and MHRD, Govt. of India for their respective fellowship. We acknowledge Dr. Sachchidanand for useful discussions. Mr. Sushanth Pradhan (Biotechnology and Medical Engineering department, NIT Rourkela) is gratefully acknowledged for technical assistance in confocal microscopy experiment. The authors also acknowledge Anthem Biosciences, Bangalore for pharmacokinetics studies. The technical help provided by Mr. Rajesh and Mr. Sher Singh is highly acknowledged.

Competing interests

The authors declare no competing interests

References

1. **WHO.** 2017. Global tuberculosis report 2017, p. 157. World Health Organization, Geneva.
2. **Russell DG.** 2007. Who puts the tubercle in tuberculosis? Nature reviews. Microbiology **5:**39-47.
3. **Bates M, Marais BJ, Zumla A.** 2015. Tuberculosis Comorbidity with Communicable and Noncommunicable Diseases. Cold Spring Harbor perspectives in medicine **5**.
4. **Chan ED, Iseman MD.** 2008. Multidrug-resistant and extensively drug-resistant tuberculosis: a review. Current opinion in infectious diseases **21:**587-595.
5. **Zumla AI, Gillespie SH, Hoelscher M, Philips PP, Cole ST, Abubakar I, McHugh TD, Schito M, Maeurer M, Nunn AJ.** 2014. New antituberculosis drugs, regimens, and adjunct therapies: needs, advances, and future prospects. The Lancet. Infectious diseases **14:**327-340.
6. **Dhiman R, Singh R.** 2018. Recent advances for identification of new scaffolds and drug targets for Mycobacterium tuberculosis. IUBMB life **70:**905-916.
7. **Manjunatha UH, Smith PW.** 2015. Perspective: Challenges and opportunities in TB drug discovery from phenotypic screening. Bioorganic & medicinal chemistry **23:**5087-5097.
8. **Mdluli K, Kaneko T, Upton A.** 2014. Tuberculosis drug discovery and emerging targets. Annals of the New York Academy of Sciences **1323:**56-75.
9. **Koul A, Arnoult E, Lounis N, Guillemont J, Andries K.** 2011. The challenge of new drug discovery for tuberculosis. Nature **469:**483-490.
10. **Singh R, Manjunatha U, Boshoff HI, Ha YH, Niyomrattanakit P, Ledwidge R, Dowd CS, Lee IY, Kim P, Zhang L, Kang S, Keller TH, Jiricek J, Barry CE, 3rd.** 2008. PA-824 kills nonreplicating Mycobacterium tuberculosis by intracellular NO release. Science **322:**1392-1395.
11. **Matsumoto M, Hashizume H, Tomishige T, Kawasaki M, Tsubouchi H, Sasaki H, Shimokawa Y, Komatsu M.** 2006. OPC-67683, a nitro-dihydro-imidazooxazole derivative with promising action against tuberculosis in vitro and in mice. PLoS medicine **3:**e466.
12. **Andries K, Verhasselt P, Guillemont J, Gohlmann HW, Neefs JM, Winkler H, Van Gestel J, Timmerman P, Zhu M, Lee E, Williams P, de Chaffoy D, Huitric E, Hoffner S, Cambau E, Truffot-Pernot C, Lounis N, Jarlier V.** 2005. A diarylquinoline drug active on the ATP synthase of Mycobacterium tuberculosis. Science **307:**223-227.
13. **Makarov V, Manina G, Mikusova K, Mollmann U, Ryabova O, Saint-Joanis B, Dhar N, Pasca MR, Buroni S, Lucarelli AP, Milano A, De Rossi E, Belanova M, Bobovska A, Dianiskova P, Kordulakova J, Sala C, Fullam E, Schneider P, McKinney JD, Brodin P, Christophe T, Waddell S, Butcher P, Albrethsen J, Rosenkrands I, Brosch R, Nandi V, Bharath S, Gaonkar S, Shandil RK, Balasubramanian V, Balganesh T, Tyagi S, Grosset J, Riccardi G, Cole ST.** 2009. Benzothiazinones kill Mycobacterium tuberculosis by blocking arabinan synthesis. Science **324:**801-804.
14. **Pethe K, Bifani P, Jang J, Kang S, Park S, Ahn S, Jiricek J, Jung J, Jeon HK, Cechetto J, Christophe T, Lee H, Kempf M, Jackson M, Lenaerts AJ, Pham H, Jones V, Seo MJ, Kim YM, Seo M, Seo JJ, Park D, Ko Y, Choi I, Kim R, Kim SY, Lim S, Yim SA, Nam J, Kang H, Kwon H, Oh CT, Cho Y, Jang Y, Kim J, Chua A, Tan BH, Nanjundappa MB, Rao SP, Barnes WS, Wintjens R, Walker JR,**

Alonso S, Lee S, Kim J, Oh S, Oh T, Nehrbass U, Han SJ, No Z, Lee J, Brodin P, Cho SN, Nam K, Kim J. 2013. Discovery of Q203, a potent clinical candidate for the treatment of tuberculosis. Nature medicine **19:**1157-1160.

15. **Tahlan K, Wilson R, Kastrinsky DB, Arora K, Nair V, Fischer E, Barnes SW, Walker JR, Alland D, Barry CE, 3rd, Boshoff HI.** 2012. SQ109 targets MmpL3, a membrane transporter of trehalose monomycolate involved in mycolic acid donation to the cell wall core of Mycobacterium tuberculosis. Antimicrobial agents and chemotherapy **56:**1797-1809.
16. **Cox E, Laessig K.** 2014. FDA approval of bedaquiline--the benefit-risk balance for drug-resistant tuberculosis. The New England journal of medicine **371:**689-691.
17. **Xavier AS, Lakshmanan M.** 2014. Delamanid: A new armor in combating drug-resistant tuberculosis. Journal of pharmacology & pharmacotherapeutics **5:**222-224.
18. **Kidwai S, Park CY, Mawatwal S, Tiwari P, Jung MG, Gosain TP, Kumar P, Alland D, Kumar S, Bajaj A, Hwang YK, Song CS, Dhiman R, Lee IY, Singh R.** 2017. Dual Mechanism of Action of 5-Nitro-1,10-Phenanthroline against Mycobacterium tuberculosis. Antimicrobial agents and chemotherapy **61**.
19. **Gupta M, Sajid A, Sharma K, Ghosh S, Arora G, Singh R, Nagaraja V, Tandon V, Singh Y.** 2014. HupB, a nucleoid-associated protein of Mycobacterium tuberculosis, is modified by serine/threonine protein kinases in vivo. Journal of bacteriology **196:**2646-2657.
20. **Arora G, Sajid A, Gupta M, Bhaduri A, Kumar P, Basu-Modak S, Singh Y.** 2010. Understanding the role of PknJ in Mycobacterium tuberculosis: biochemical characterization and identification of novel substrate pyruvate kinase A. PloS one **5:**e10772.
21. **Gilson MK, Liu T, Baitaluk M, Nicola G, Hwang L, Chong J.** 2016. BindingDB in 2015: A public database for medicinal chemistry, computational chemistry and systems pharmacology. Nucleic acids research **44:**D1045-1053.
22. **Kim S, Thiessen PA, Bolton EE, Chen J, Fu G, Gindulyte A, Han L, He J, He S, Shoemaker BA, Wang J, Yu B, Zhang J, Bryant SH.** 2016. PubChem Substance and Compound databases. Nucleic acids research **44:**D1202-1213.
23. **Wishart DS, Feunang YD, Guo AC, Lo EJ, Marcu A, Grant JR, Sajed T, Johnson D, Li C, Sayeeda Z, Assempour N, Iynkkaran I, Liu Y, Maciejewski A, Gale N, Wilson A, Chin L, Cummings R, Le D, Pon A, Knox C, Wilson M.** 2018. DrugBank 5.0: a major update to the DrugBank database for 2018. Nucleic acids research **46:**D1074-D1082.
24. **Rosenthal LS, Drake D, Alcalay RN, Babcock D, Bowman FD, Chen-Plotkin A, Dawson TM, Dewey RB, Jr., German DC, Huang X, Landin B, McAuliffe M, Petyuk VA, Scherzer CR, Hillaire-Clarke CS, Sieber BA, Sutherland M, Tarn C, West A, Vaillancourt D, Zhang J, Gwinn K, consortium P.** 2016. The NINDS Parkinson's disease biomarkers program. Movement disorders : official journal of the Movement Disorder Society **31:**915-923.
25. **Arris CE, Boyle FT, Calvert AH, Curtin NJ, Endicott JA, Garman EF, Gibson AE, Golding BT, Grant S, Griffin RJ, Jewsbury P, Johnson LN, Lawrie AM, Newell DR, Noble ME, Sausville EA, Schultz R, Yu W.** 2000. Identification of novel purine and pyrimidine cyclin-dependent kinase inhibitors with distinct molecular interactions and tumor cell growth inhibition profiles. Journal of medicinal chemistry **43:**2797-2804.

807 26. **Berman HM, Westbrook J, Feng Z, Gilliland G, Bhat TN, Weissig H,**
808 **Shindyalov IN, Bourne PE.** 2000. The Protein Data Bank. Nucleic acids research
809 **28:**235-242.
810 27. **Scherr N, Honnappa S, Kunz G, Mueller P, Jayachandran R, Winkler F,**
811 **Pieters J, Steinmetz MO.** 2007. Structural basis for the specific inhibition of
812 protein kinase G, a virulence factor of Mycobacterium tuberculosis. Proceedings
813 of the National Academy of Sciences of the United States of America **104:**12151-
814 12156.
815 28. **Ortiz-Lombardia M, Pompeo F, Boitel B, Alzari PM.** 2003. Crystal structure of
816 the catalytic domain of the PknB serine/threonine kinase from Mycobacterium
817 tuberculosis. The Journal of biological chemistry **278:**13094-13100.
818 29. **Wehenkel A, Fernandez P, Bellinzoni M, Catherinot V, Barilone N, Labesse**
819 **G, Jackson M, Alzari PM.** 2006. The structure of PknB in complex with
820 mitoxantrone, an ATP-competitive inhibitor, suggests a mode of protein kinase
821 regulation in mycobacteria. FEBS letters **580:**3018-3022.
822 30. **Young TA, Delagoutte B, Endrizzi JA, Falick AM, Alber T.** 2003. Structure of
823 Mycobacterium tuberculosis PknB supports a universal activation mechanism
824 for Ser/Thr protein kinases. Nature structural biology **10:**168-174.
825 31. **Sastry GM, Adzhigirey M, Day T, Annabhimoju R, Sherman W.** 2013. Protein
826 and ligand preparation: parameters, protocols, and influence on virtual
827 screening enrichments. Journal of computer-aided molecular design **27:**221-234.
828 32. **Harder E, Damm W, Maple J, Wu C, Reboul M, Xiang JY, Wang L, Lupyan D,**
829 **Dahlgren MK, Knight JL, Kaus JW, Cerutti DS, Krilov G, Jorgensen WL, Abel**
830 **R, Friesner RA.** 2016. OPLS3: A Force Field Providing Broad Coverage of Drug-
831 like Small Molecules and Proteins. Journal of chemical theory and computation
832 **12:**281-296.
833 33. **Ravala SK, Singh S, Yadav GS, Kumar S, Karthikeyan S, Chakraborti PK.**
834 2015. Evidence that phosphorylation of threonine in the GT motif triggers
835 activation of PknA, a eukaryotic-type serine/threonine kinase from
836 Mycobacterium tuberculosis. The FEBS journal **282:**1419-1431.
837 34. **Mieczkowski C, Iavarone AT, Alber T.** 2008. Auto-activation mechanism of the
838 Mycobacterium tuberculosis PknB receptor Ser/Thr kinase. The EMBO journal
839 **27:**3186-3197.
840 35. **Roos K, Wu C, Damm W, Reboul M, Stevenson JM, Lu C, Dahlgren MK,**
841 **Mondal S, Chen W, Wang L, Abel R, Friesner RA, Harder ED.** 2019. OPLS3e:
842 Extending Force Field Coverage for Drug-Like Small Molecules. Journal of
843 chemical theory and computation **15:**1863-1874.
844 36. **Riveiro-Falkenbach E, Ruano Y, Garcia-Martin RM, Lora D, Cifdaloz M,**
845 **Acquadro F, Ballestin C, Ortiz-Romero PL, Soengas MS, Rodriguez-Peralto**
846 **JL.** 2016. DEK oncogene is overexpressed during melanoma progression.
847 Pigment cell & melanoma research.
848 37. **Sherman W, Day T, Jacobson MP, Friesner RA, Farid R.** 2006. Novel procedure
849 for modeling ligand/receptor induced fit effects. Journal of medicinal chemistry
850 **49:**534-553.
851 38. **Bissantz C, Kuhn B, Stahl M.** 2010. A medicinal chemist's guide to molecular
852 interactions. Journal of medicinal chemistry **53:**5061-5084.
853 39. **Jacobson MP, Friesner RA, Xiang Z, Honig B.** 2002. On the role of the crystal
854 environment in determining protein side-chain conformations. Journal of
855 molecular biology **320:**597-608.

40. **Jacobson MP, Pincus DL, Rapp CS, Day TJ, Honig B, Shaw DE, Friesner RA.** 2004. A hierarchical approach to all-atom protein loop prediction. Proteins **55:**351-367.
41. **Laskowski RA, Rullmannn JA, MacArthur MW, Kaptein R, Thornton JM.** 1996. AQUA and PROCHECK-NMR: programs for checking the quality of protein structures solved by NMR. Journal of biomolecular NMR **8:**477-486.
42. **Li W, Cowley A, Uludag M, Gur T, McWilliam H, Squizzato S, Park YM, Buso N, Lopez R.** 2015. The EMBL-EBI bioinformatics web and programmatic tools framework. Nucleic acids research **43:**W580-584.
43. **Robert X, Gouet P.** 2014. Deciphering key features in protein structures with the new ENDscript server. Nucleic acids research **42:**W320-324.
44. **Pei J, Kim BH, Grishin NV.** 2008. PROMALS3D: a tool for multiple protein sequence and structure alignments. Nucleic acids research **36:**2295-2300.
45. **Mawatwal S, Behura A, Ghosh A, Kidwai S, Mishra A, Deep A, Agarwal S, Saha S, Singh R, Dhiman R.** 2017. Calcimycin mediates mycobacterial killing by inducing intracellular calcium-regulated autophagy in a P2RX7 dependent manner. Biochimica et biophysica acta **1861:**3190-3200.
46. **Garnier T, Eiglmeier K, Camus JC, Medina N, Mansoor H, Pryor M, Duthoy S, Grondin S, Lacroix C, Monsempe C, Simon S, Harris B, Atkin R, Doggett J, Mayes R, Keating L, Wheeler PR, Parkhill J, Barrell BG, Cole ST, Gordon SV, Hewinson RG.** 2003. The complete genome sequence of Mycobacterium bovis. Proceedings of the National Academy of Sciences of the United States of America **100:**7877-7882.
47. **Ballell L, Bates RH, Young RJ, Alvarez-Gomez D, Alvarez-Ruiz E, Barroso V, Blanco D, Crespo B, Escribano J, Gonzalez R, Lozano S, Huss S, Santos-Villarejo A, Martin-Plaza JJ, Mendoza A, Rebollo-Lopez MJ, Remuinan-Blanco M, Lavandera JL, Perez-Herran E, Gamo-Benito FJ, Garcia-Bustos JF, Barros D, Castro JP, Cammack N.** 2013. Fueling open-source drug discovery: 177 small-molecule leads against tuberculosis. ChemMedChem **8:**313-321.
48. **Altaf M, Miller CH, Bellows DS, O'Toole R.** 2010. Evaluation of the Mycobacterium smegmatis and BCG models for the discovery of Mycobacterium tuberculosis inhibitors. Tuberculosis **90:**333-337.
49. **Mawatwal S, Behura A, Mishra A, Singh R, Dhiman R.** 2018. Calcimycin induced IL-12 production inhibits intracellular mycobacterial growth by enhancing autophagy. Cytokine **111:**1-12.
50. **Pandey M, Singh AK, Thakare R, Talwar S, Karaulia P, Dasgupta A, Chopra S, Pandey AK.** 2017. Diphenyleneiodonium chloride (DPIC) displays broad-spectrum bactericidal activity. Scientific reports **7:**11521.
51. **Prisic S, Husson RN.** 2014. Mycobacterium tuberculosis Serine/Threonine Protein Kinases. Microbiology spectrum **2**.
52. **Lisa MN, Gil M, Andre-Leroux G, Barilone N, Duran R, Biondi RM, Alzari PM.** 2015. Molecular Basis of the Activity and the Regulation of the Eukaryotic-like S/T Protein Kinase PknG from Mycobacterium tuberculosis. Structure **23:**1039-1048.
53. **Manning G, Whyte DB, Martinez R, Hunter T, Sudarsanam S.** 2002. The protein kinase complement of the human genome. Science **298:**1912-1934.
54. **Ehrt S, Schnappinger D.** 2009. Mycobacterial survival strategies in the phagosome: defence against host stresses. Cellular microbiology **11:**1170-1178.

55. **Queval CJ, Brosch R, Simeone R.** 2017. The Macrophage: A Disputed Fortress in the Battle against Mycobacterium tuberculosis. Frontiers in microbiology **8:**2284.
56. **Deretic V.** 2014. Autophagy in tuberculosis. Cold Spring Harbor perspectives in medicine **4:**a018481.
57. **Parandhaman DK, Narayanan S.** 2014. Cell death paradigms in the pathogenesis of Mycobacterium tuberculosis infection. Frontiers in cellular and infection microbiology **4:**31.
58. **Peasland A, Wang LZ, Rowling E, Kyle S, Chen T, Hopkins A, Cliby WA, Sarkaria J, Beale G, Edmondson RJ, Curtin NJ.** 2011. Identification and evaluation of a potent novel ATR inhibitor, NU6027, in breast and ovarian cancer cell lines. British journal of cancer **105:**372-381.
59. **Sultana R, Abdel-Fatah T, Perry C, Moseley P, Albarakti N, Mohan V, Seedhouse C, Chan S, Madhusudan S.** 2013. Ataxia telangiectasia mutated and Rad3 related (ATR) protein kinase inhibition is synthetically lethal in XRCC1 deficient ovarian cancer cells. PloS one **8:**e57098.
60. **Spira A, Carroll JD, Liu G, Aziz Z, Shah V, Kornfeld H, Keane J.** 2003. Apoptosis genes in human alveolar macrophages infected with virulent or attenuated Mycobacterium tuberculosis: a pivotal role for tumor necrosis factor. American journal of respiratory cell and molecular biology **29:**545-551.
61. **Ehrhardt H, Hofig I, Wachter F, Obexer P, Fulda S, Terziyska N, Jeremias I.** 2012. NOXA as critical mediator for drug combinations in polychemotherapy. Cell death & disease **3:**e327.
62. **Pradhan G, Shrivastva R, Mukhopadhyay S.** 2018. Mycobacterial PknG Targets the Rab7l1 Signaling Pathway To Inhibit Phagosome-Lysosome Fusion. Journal of immunology **201:**1421-1433.
63. **Koul A, Choidas A, Tyagi AK, Drlica K, Singh Y, Ullrich A.** 2001. Serine/threonine protein kinases PknF and PknG of Mycobacterium tuberculosis: characterization and localization. Microbiology **147:**2307-2314.
64. **Khan MZ, Bhaskar A, Upadhyay S, Kumari P, Rajmani RS, Jain P, Singh A, Kumar D, Bhavesh NS, Nandicoori VK.** 2017. Protein kinase G confers survival advantage to Mycobacterium tuberculosis during latency-like conditions. The Journal of biological chemistry **292:**16093-16108.
65. **Molloy A, Laochumroonvorapong P, Kaplan G.** 1994. Apoptosis, but not necrosis, of infected monocytes is coupled with killing of intracellular bacillus Calmette-Guerin. The Journal of experimental medicine **180:**1499-1509.
66. **Schaible UE, Winau F, Sieling PA, Fischer K, Collins HL, Hagens K, Modlin RL, Brinkmann V, Kaufmann SH.** 2003. Apoptosis facilitates antigen presentation to T lymphocytes through MHC-I and CD1 in tuberculosis. Nature medicine **9:**1039-1046.
67. **Behar SM, Martin CJ, Booty MG, Nishimura T, Zhao X, Gan HX, Divangahi M, Remold HG.** 2011. Apoptosis is an innate defense function of macrophages against Mycobacterium tuberculosis. Mucosal immunology **4:**279-287.
68. **Chen D, Ma S, He L, Yuan P, She Z, Lu Y.** 2017. Sclerotiorin inhibits protein kinase G from Mycobacterium tuberculosis and impairs mycobacterial growth in macrophages. Tuberculosis **103:**37-43.
69. **Janssen S, Jayachandran R, Khathi L, Zinsstag J, Grobusch MP, Pieters J.** 2012. Exploring prospects of novel drugs for tuberculosis. Drug design, development and therapy **6:**217-224.

70. **Kanehiro Y, Tomioka H, Pieters J, Tatano Y, Kim H, Iizasa H, Yoshiyama H.** 2018. Identification of Novel Mycobacterial Inhibitors Against Mycobacterial Protein Kinase G. Frontiers in microbiology **9:**1517.

71. **Singh N, Tiwari S, Srivastava KK, Siddiqi MI.** 2015. Identification of Novel Inhibitors of Mycobacterium tuberculosis PknG Using Pharmacophore Based Virtual Screening, Docking, Molecular Dynamics Simulation, and Their Biological Evaluation. Journal of chemical information and modeling **55:**1120-1129.

72. **Slee EA, Zhu H, Chow SC, MacFarlane M, Nicholson DW, Cohen GM.** 1996. Benzyloxycarbonyl-Val-Ala-Asp (OMe) fluoromethylketone (Z-VAD.FMK) inhibits apoptosis by blocking the processing of CPP32. The Biochemical journal **315 (Pt 1):**21-24.

73. **Charrier JD, Durrant SJ, Golec JM, Kay DP, Knegtel RM, MacCormick S, Mortimore M, O'Donnell ME, Pinder JL, Reaper PM, Rutherford AP, Wang PS, Young SC, Pollard JR.** 2011. Discovery of potent and selective inhibitors of ataxia telangiectasia mutated and Rad3 related (ATR) protein kinase as potential anticancer agents. Journal of medicinal chemistry **54:**2320-2330.

74. **Chapman TM, Bouloc N, Buxton RS, Chugh J, Lougheed KE, Osborne SA, Saxty B, Smerdon SJ, Taylor DL, Whalley D.** 2012. Substituted aminopyrimidine protein kinase B (PknB) inhibitors show activity against Mycobacterium tuberculosis. Bioorganic & medicinal chemistry letters **22:**3349-3353.

75. **Punkvang A, Hannongbua S, Saparpakorn P, Pungpo P.** 2016. Insight into the structural requirements of aminopyrimidine derivatives for good potency against both purified enzyme and whole cells of M. tuberculosis: combination of HQSAR, CoMSIA, and MD simulation studies. Journal of biomolecular structure & dynamics **34:**1079-1091.

76. **Khan MZ, Kaur P, Nandicoori VK.** 2018. Targeting the messengers: Serine/threonine protein kinases as potential targets for antimycobacterial drug development. IUBMB life **70:**889-904.

77. **Parish T.** 2014. Two-Component Regulatory Systems of Mycobacteria. Microbiology spectrum **2:**MGM2-0010-2013.

78. **Nagarajan SN, Upadhyay S, Chawla Y, Khan S, Naz S, Subramanian J, Gandotra S, Nandicoori VK.** 2015. Protein kinase A (PknA) of Mycobacterium tuberculosis is independently activated and is critical for growth in vitro and survival of the pathogen in the host. The Journal of biological chemistry **290:**9626-9645.

79. **Chawla Y, Upadhyay S, Khan S, Nagarajan SN, Forti F, Nandicoori VK.** 2014. Protein kinase B (PknB) of Mycobacterium tuberculosis is essential for growth of the pathogen in vitro as well as for survival within the host. The Journal of biological chemistry **289:**13858-13875.

80. **Bhattacharyya N, Nkumama IN, Newland-Smith Z, Lin LY, Yin W, Cullen RE, Griffiths JS, Jarvis AR, Price MJ, Chong PY, Wallis R, O'Hare HM.** 2018. An Aspartate-Specific Solute-Binding Protein Regulates Protein Kinase G Activity To Control Glutamate Metabolism in Mycobacteria. mBio **9**.

81. **Walburger A, Koul A, Ferrari G, Nguyen L, Prescianotto-Baschong C, Huygen K, Klebl B, Thompson C, Bacher G, Pieters J.** 2004. Protein kinase G from pathogenic mycobacteria promotes survival within macrophages. Science **304:**1800-1804.

1001 82. **Hatzios SK, Baer CE, Rustad TR, Siegrist MS, Pang JM, Ortega C, Alber T,**
1002 **Grundner C, Sherman DR, Bertozzi CR.** 2013. Osmosensory signaling in
1003 Mycobacterium tuberculosis mediated by a eukaryotic-like Ser/Thr protein
1004 kinase. Proceedings of the National Academy of Sciences of the United States of
1005 America **110:**E5069-5077.
1006 83. **Be NA, Bishai WR, Jain SK.** 2012. Role of Mycobacterium tuberculosis pknD in
1007 the pathogenesis of central nervous system tuberculosis. BMC microbiology
1008 **12:**7.
1009 84. **Briken V, Miller JL.** 2008. Living on the edge: inhibition of host cell apoptosis by
1010 Mycobacterium tuberculosis. Future microbiology **3:**415-422.
1011 85. **Huang J, Jiao J, Xu W, Zhao H, Zhang C, Shi Y, Xiao Z.** 2015. MiR-155 is
1012 upregulated in patients with active tuberculosis and inhibits apoptosis of
1013 monocytes by targeting FOXO3. Molecular medicine reports **12:**7102-7108.
1014 86. **Xi X, Zhang C, Han W, Zhao H, Zhang H, Jiao J.** 2015. MicroRNA-223 Is
1015 Upregulated in Active Tuberculosis Patients and Inhibits Apoptosis of
1016 Macrophages by Targeting FOXO3. Genetic testing and molecular biomarkers
1017 **19:**650-656.
1018

1019

1020 **Figure Legends**

1021 **Figure 1: (A)** Structures of the identified lead compound NU-6027. **(B-D)** Structures of the
1022 synthesized NU-6027 derivatives. **(E and F)** For *in vitro* experiments, early-log phase culture
1023 of *M. bovis* BCG was exposed to either NU-6027 or INH. For bacterial enumeration, cultures
1024 were diluted 10.0 fold and 100 µl was plated on MB7H11 plates. The data shown in this
1025 panel is mean ± S.E. of bacterial counts at designated time points. The data shown is
1026 representative of two independent experiments. Significant differences were obtained for the
1027 indicated groups (paired (two-tailed) t-test, *$p<0.05$ and **$p<0.01$).

1028 **Figure 2: *In vitro* autophosphorylation assays of STPK's in the presence or absence of**
1029 **NU-6027. (A)** STPK's enzymes (as indicated) were purified and activity assays were
1030 performed in the presence or absence of NU-6027 as described in Materials and methods.
1031 STPK activity inhibition was tested at either 100 µM (1) or 50 µM (2) NU-6027
1032 concentration. All reactions included no enzyme control. The reactions were analysed by
1033 autoradiography and SDS-PAGE analysis as indicated. **(B)** *In vitro* autophosphorylation
1034 assays of PknD and PknG were performed in the indicated concentrations of NU-6027.

1035 **Figure 3: Interaction profile of NU-6027 in binding sites of *M. tuberculosis* PknG, PknB,**
1036 **PknD and PknA. (A)** This panel represents interaction between PknG and docked pose of
1037 NU-6027. The PknG specific residues are labelled in blue color. **(B)** This panel depicts
1038 interaction between PknB and docked pose of NU-6027. **(C)** This panel represents interaction
1039 between PknD model and docked NU-6027. **(D)** This panel depicts interaction between PknA
1040 and docked NU-6027. In all the panels, the protein residues (without the non-polar hydrogen
1041 atoms) involved in hydrogen bonding are shown as thin sticks (black carbon atoms) and their
1042 labels have been encircled in green outline. The functional residues in hinge region are
1043 encircled in brown outline if they are engaged in hydrogen bonding with the ligand else they
1044 are labelled in brown font. The hydrogen bonds in all panels are shown as green broken lines.
1045 The Cα atoms of the amino acids residues (apart from the ones which are involved in
1046 hydrogen bonding) within 5Å of the predicted pose NU-6027 have been shown as black
1047 small spheres. The remaining atoms of the binding site residues and non-polar hydrogens of
1048 ligand have not been shown for better visual clarity.

1049 **Figure 4: Comparative analysis of binding poses of NU-6027 in STPKs. (A)** Overlay of
1050 the docked pose of NU-6027 in PknG (pink) and, PknB (cyan) on to its bound pose in CDK2
1051 (green). The black circle highlights that pyrimidine ring of NU-6027 occupies topologically
1052 almost equivalent regions in PknG and CDK2. The black arrows indicate that the cyclohexyl

1053 ring of NU-6027 occupies topologically non-equivalent region in CDK2 and PknG. The area
1054 highlighted in red rectangle shows that the pyrimidine and cyclohexyl ring of NU-6027 are
1055 almost flipped by 180° in PknB in comparison to their orientation in CDK2. **(B)** The panel
1056 represents the overlay of the docked pose of NU-6027 in PknD (violet) and PknA onto PknG
1057 (pink). The black circle highlights that the pyrimidine ring of NU-6027 occupies almost
1058 topologically equivalent regions in the respective proteins. **(C-D)** These panels represent the
1059 predicted pose of NU-6027 in PknA (C) and PknG (D) binding site. The Cα atoms of the
1060 residues lying within 4Å of the carbon atoms of cyclohexyl ring are shown as orange spheres.
1061 The labels of the unique residues of PknG are shown in blue font. The atoms of cyclohexyl
1062 ring of docked NU-6027 in PknA shown in cyan color are solvent exposed. The
1063 corresponding atoms of docked NU-6027 in PknG are shielded from solvent by the amino
1064 terminus segment comprising of unique residues Ile87 and Ala92 and Gly236 from kinase
1065 domain.

1066 **Figure 5: Apoptosis in *M. bovis* BCG infected THP-1 macrophages upon NU-6027**
1067 **treatment. (A)** THP-1 macrophages were infected with either *M. bovis* BCG as discussed in
1068 Materials and methods. Uninfected or infected THP-1 macrophages were treated with 25 μM
1069 NU-6027. After 24 hrs of treatment, apoptosis of macrophages was quantified using
1070 Annexin-V staining as described in Materials and methods. The numbers shown in each
1071 quadrant depicts the percentage of stained cells. The data shown in this panel is
1072 representative images obtained from three independent experiments. **(B)** For qPCR analysis,
1073 mRNA was isolated, cDNA was synthesized, and the transcripts levels of the indicated
1074 apoptosis related genes were quantified. The data shown in this panel is fold change in
1075 expression levels after normalization to the expression of housekeeping gene, GAPDH. The
1076 values shown in this panel is mean ± S.E. of fold change obtained from 2 experiments
1077 performed in triplicate wells. Significant differences were obtained for the indicated groups
1078 (paired (two-tailed) t-test, *$p<0.05$). **(C-D) NU-6027 inhibits mycobacterial growth in**
1079 **THP-1 macrophages.** THP-1 macrophages were infected with either *M. bovis* BCG (C) or
1080 *M. tuberculosis* (D) at a MOI of 1:10. At 24 hrs post-infection, macrophages were overlaid
1081 with RPMI medium containing 25 μM NU-6027. After 4 days of treatment, macrophages
1082 were lysed and dilutions were plated on MB7H11 plates. Significant differences were
1083 obtained for the indicated groups (paired (two-tailed) t-test, *$p<0.05$ and **$p<0.01$).

1084 **Figure 6: Z-VAD-FMK inhibits apoptosis in *M. bovis* BCG infected THP-1**
1085 **macrophages upon NU-6027 treatment. (A)** THP-1 macrophages were pre-incubated with

1086 20 μM Z-VAD-FMK. After 2 hrs of incubation, THP-1 macrophages were infected with *M.*
1087 *bovis* BCG as discussed in Materials and methods. Uninfected or infected THP-1
1088 macrophages were treated with 25 μM NU-6027. After 24 hrs of treatment, apoptosis of
1089 macrophages was quantified using Annexin-V staining as described in Materials and
1090 methods. The numbers shown in each quadrant depicts the percentage of stained cells. The
1091 data shown in this panel is representative images obtained from three independent
1092 experiments. **(B)** THP-1 macrophages were seeded, differentiated and pre-treated with 20 μM
1093 Z-VAD-FMK. Following, 2 hrs of pre-treatment, macrophages were infected with *M. bovis*
1094 BCG at a MOI of 1:10 and bacterial enumeration was performed as described in Materials
1095 and methods. Significant differences were obtained for the indicated groups (paired (two-
1096 tailed) t-test, *$p<0.05$).
1097 **Figure 7: NU-6027 inhibits the growth of *M. tuberculosis* in mice tissues. (A-B)**
1098 Pharmacokinetic studies of NU-6027 in BALB/c mice when orally administered daily at 100
1099 mg/kg for 5 consecutive days. **(C-D)** 4-6 weeks old female BALB/c mice were infected with
1100 *M. tuberculosis* via aerosol route. The data shown in these panels is mean ± S.E. of lung and
1101 splenic bacillary loads at 2 weeks (C) and 4 weeks (D) post-treatment. Statistical differences
1102 were obtained for the indicated groups (*$p<0.05$, **$p<0.01$ and ***$p<0.001$).
1103

1104

1105 **Table 1**: List of small molecule inhibitors identified in our screening of Sigma Lopac 1280
1106 library against *M. bovis BCG*.

1107

S. No.	Drugs	MIC_{99} (*M. bovis* BCG)	Mechanism of action 1108 1109
1.	AC-93253 iodide	1.56	RARα agonist
2.	Azithromycin	0.39	Inhibition of protein synthesis
3.	Calcimycin	1.56	Calcium ionophore
4.	Calmidazolium chloride	12.5	Inhibition of calmodulin-regulated enzymes
5.	Diphenylene iodonium chloride	<0.05	Inhibition of nitric oxide synthetase
6.	Doxycycline hydrochloride	0.39	Inhibition of matrix metalloproteinases and protein synthesis
7.	Demeclocycline hydrochloride	0.78	Inhibition of protein synthesis, suppresses calpain I and II activities
8.	Dequalinium chloride hydrate	6.25	Bactericidal and fungicidal activities
9.	Ellipticine	12.5	Inhibitor of topoisomerase II
10.	Fusidic acid	6.25	Inhibitor of translocation of peptidyl tRNA
11.	Idarubicin hydrochloride	6.25	Inhibitor of topoisomerase II
12.	Lomefloxacin hydrochloride	12.5	Inhibitor of DNA gyrase (topoisomerase II) and topoisomerase IV
13.	L-687,384 hydrochloride	12.5	σ1 receptor agonist
14.	Minocycline hydrochloride	1.56	Inhibitor of protein synthesis
15.	Methoctramine tetrahydrochloride	3.125	M2 muscarinic receptor antagonist
16.	Nialamide	12.5	Non-selective MAO-A/B inhibitor
17.	Niclosamide	12.5	Inhibits mitochondrial oxidative phosphorylation and induction of apoptosis
18.	NU-6027	1.56	Cyclin-dependent kinase 2 inhibitor
19.	Trevafloxacin mesylate	3.125	Inhibitor of DNA gyrase and topoisomerase IV
20.	4-hydroxy benzhydrazide	12.5	------

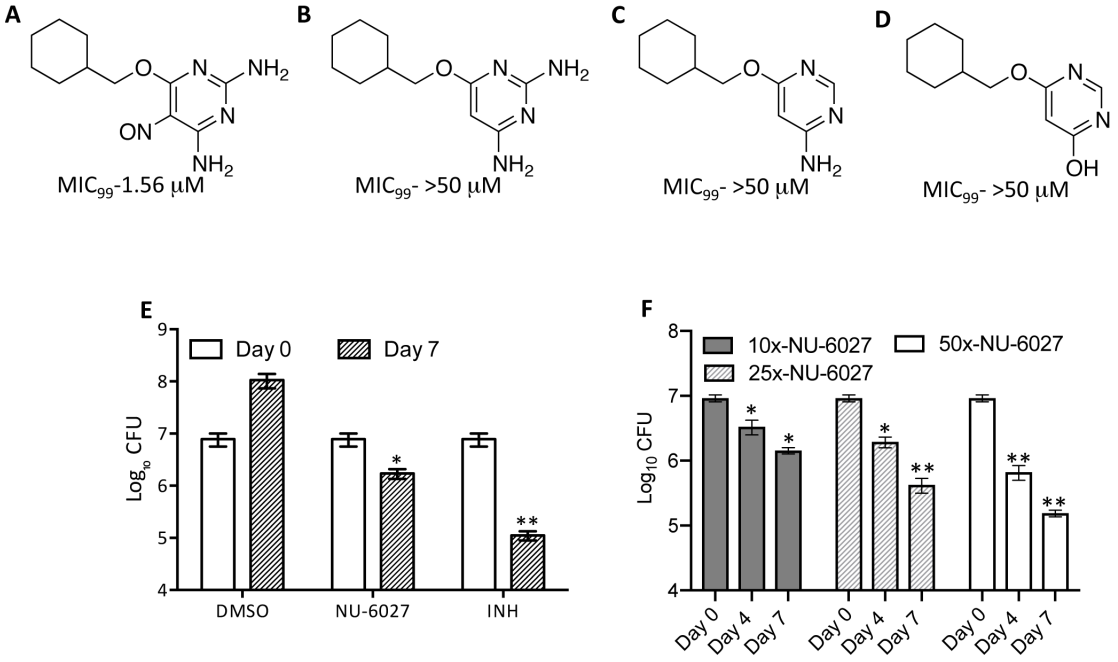

Kidwai et al., Figure 1

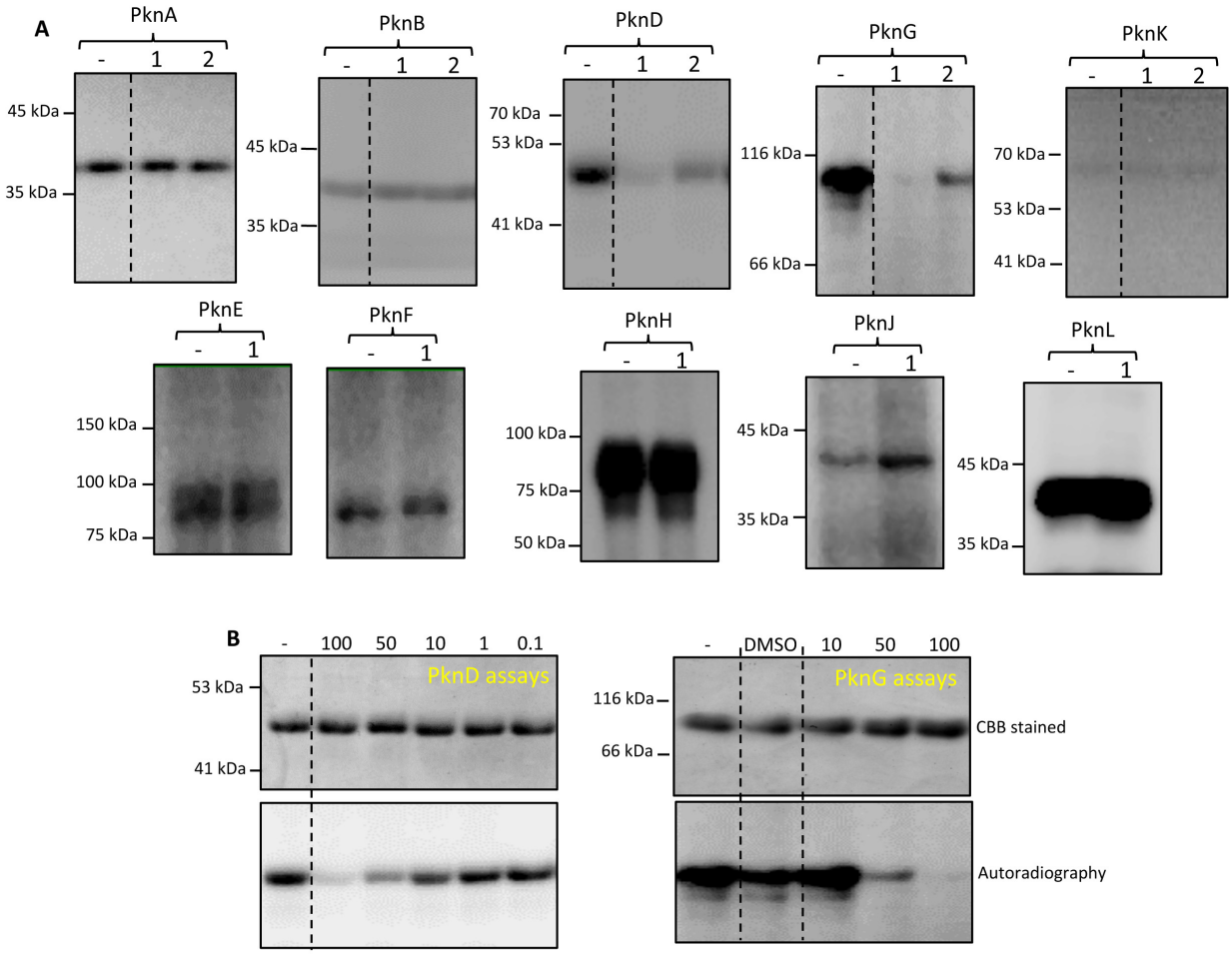

Kidwai et al., Figure 2

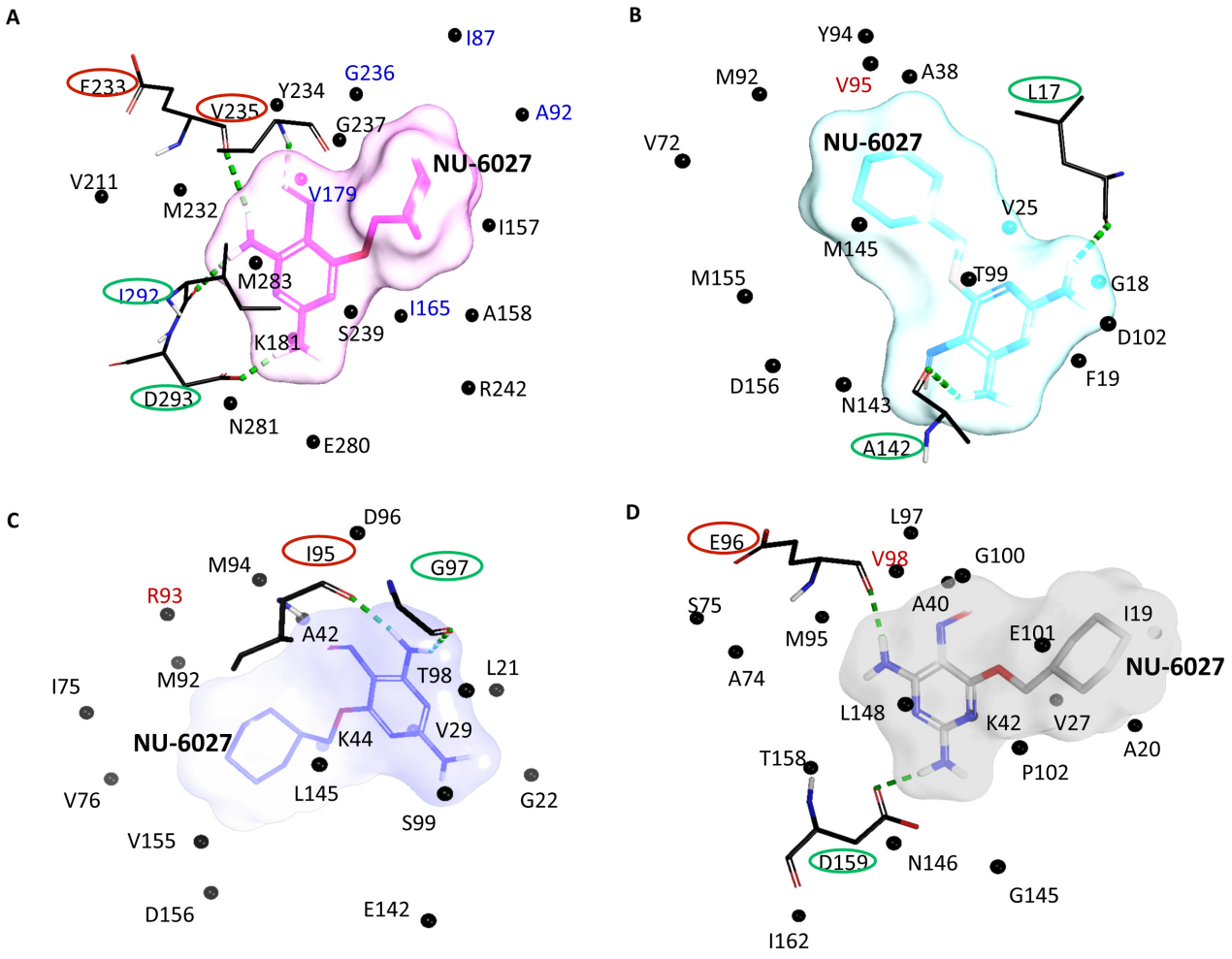

Kidwai et al., Figure 3

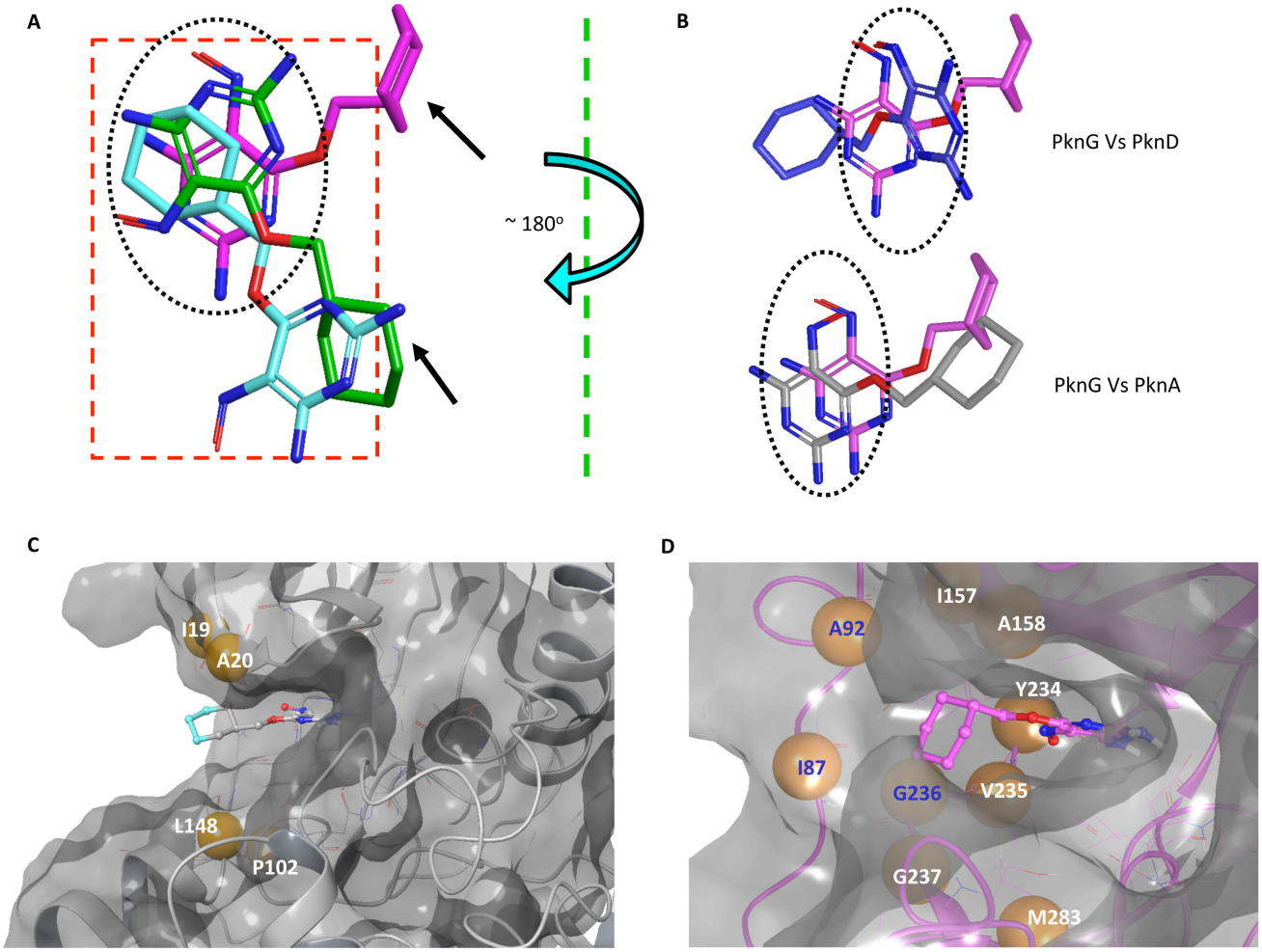

Kidwai et al., Figure 4

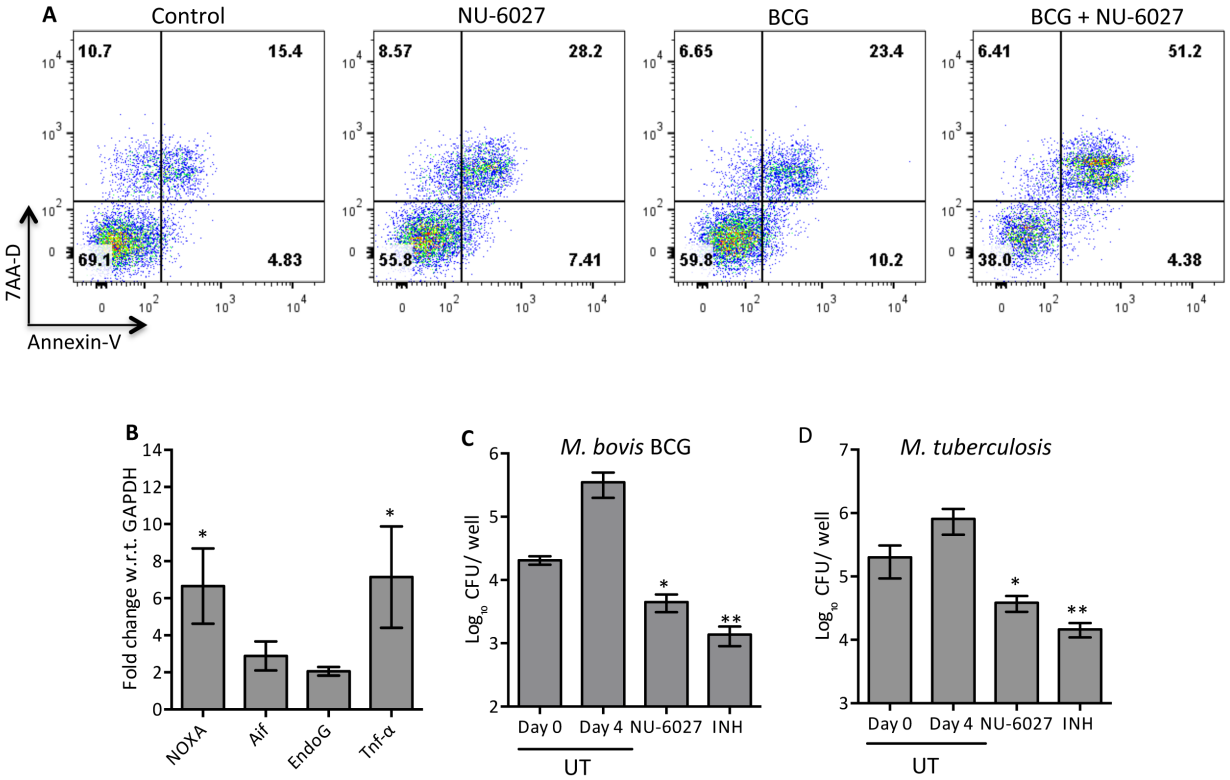

Kidwai et al., Figure 5

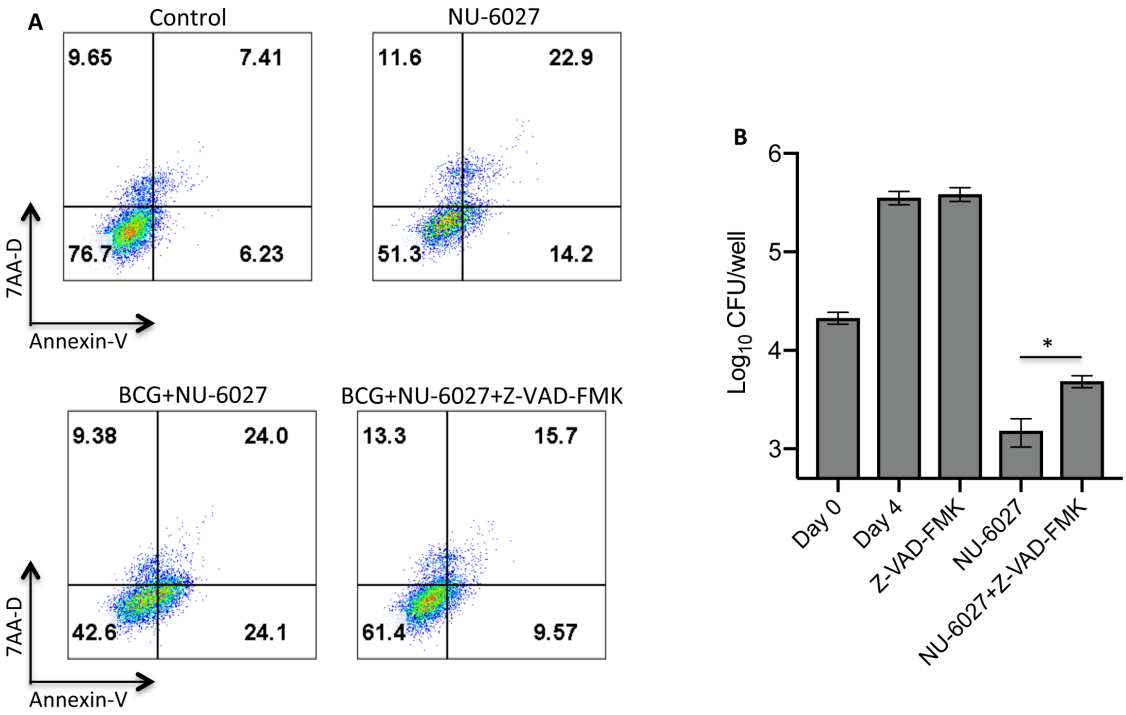

Kidwai et al., Figure 6

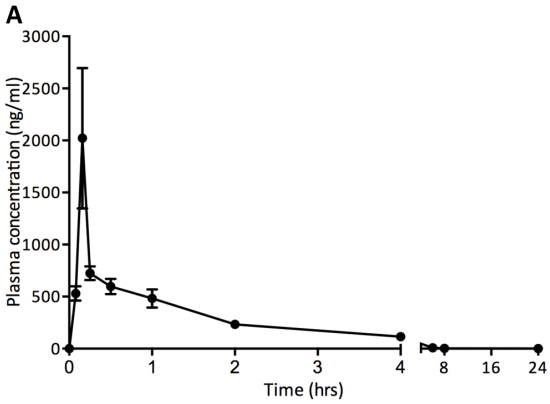

B

Paramteres	N4411
Route of administration	Oral
Dose (mg/kg)	100
Cmax (ng/ml)	2021.32
T_{max} (h)	0.16
AUC_{last} (h*ng/ml)	1526.16
AUC_{linf} (h*ng/ml)	1526.16
$T_{1/2\ (h)}$	0.96

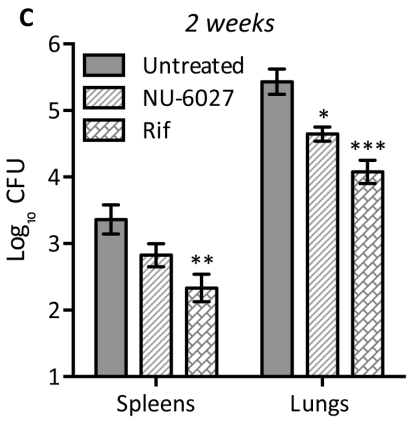

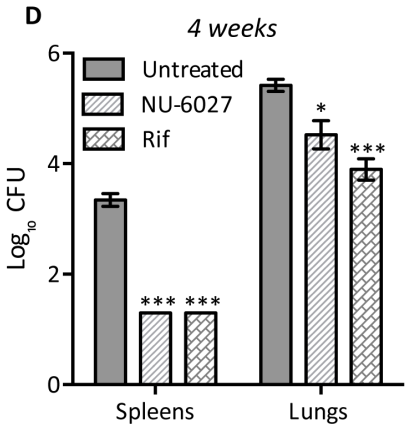

Kidwai et al., Figure 7